NATIONAL INSTITUTE FOR FUSION SCIENCE

UV and X-Ray Spectral Lines of Be-Like Fe Ion for Plasma Diagnostics

I. Murakami, T. Kato and J. Dubau

RESEARCH REPORT
NIFS-DATA Series

NAGOYA, JAPAN

UV and X-Ray Spectral Lines of Be-Like Fe Ion for Plasma Diagnostics

Izumi Murakami, Takako Kato, and Jacque Dubau *

National Institute for Fusion Science, Nagoya 464-01, Japan
* Observatory of Paris, Meudon, France

ABSTRACT

We have calculated X-ray and UV spectra of the Be-like Fe (FeXXIII) ion using collisional-radiative model including all fine-structure transitions among the $2s^2$, $2s2p$, $2p^2$, $2snl$, and $2pnl$ levels where $n = 3$ and 4, adopting data for the collision strengths by Zhang & Sampson (1992) and by Sampson, Goett, & Clark (1984). Some line intensity ratios can be used for the temperature diagnostic. We show 5 ratios in UV region and 9 ratios in X-ray region as functions of electron temperature and density at $0.3\text{keV} \lesssim T_e \lesssim 10\text{keV}$ and $n_e = 1 - 10^{25}\text{cm}^{-3}$. The effect of cascade in these line ratios is discussed.

Keywords: FeXXIII, excitation rate coefficients, population densities, spectral lines, intensity ratios, plasma diagnostics

1   Introduction

Intensity ratios of emission lines of ions can be used for plasma diagnostics. FeXXIII, Be-like Fe ion, is observed in fusion plasma at around $T_e \sim 10^7$K (1keV) as well as astrophysical plasma, such as solar corona and flares [1], and intracluster gas [2].

Historically, so-called corona model has been used to calculate level population densities to get intensities of emission lines, considered only collisional excitation from the ground state in the calculation. However, the metastable state, such as $2s2p\ ^3P$ state, plays an important role for the population density of L-shell ions even at low density region.

We have constructed a collisional-radiative model for L-shell ions, including all transitions up to $n = 4$. This model takes into account the effects of excitation from metastable states and radiative cascades from upper levels.

Bhatia & Mason [3] examined the population densities of FeXXIII, including all transitions among 20 levels, $2s^2$, $2s2p$, $2p^2$, and $2s3l$, and estimated the line intensity ratios as a function of electron temperature. Keenan et al. [4] examined the intensity ratios for transitions between $n = 2$ levels of FeXXIII for 10 levels. Since their numbers of levels considered in their calculations are small, the effect of radiative cascades to the population densities is underestimated.

Here, we calculate the population density of Be-like Fe ion by the collisional-radiative model, including all transitions among 98 levels of $2s^2$, $2s2p$, $2p^2$, $2snl$, and $2pnl$ ($n \leq 4$) with different data from the previous authors for collision strengths given by Zhang and Sampson [5], and Sampson, Goett, and Clark [6]. Using the results, we study the line intensity ratios as functions of electron temperature and density for plasma diagnostics. We discuss the effect of the metastable state and the radiative cascades from upper levels to the population density as well as the line intensity ratio.

2 Atomic Data

The fine structure energy levels and transition probabilities are calculated by AUTOLSJ method (Dubau et al. [7]) with SUPERSTRUCTURE Code for the principal quantum number $n \leq 4$, and 98 levels of the $1s^2 2snl$ and $1s^2 2pnl$ configurations are considered. The configurations and the energies of all the levels considered are listed in Table 1 and the transition probabilities and wavelengths of all transitions are listed in Table 2. We have also included a magnetic quadrapole transition probability for $2s^2 \, {}^1S_0 - 2s2p \, {}^3P_2$ as 7.51 s^{-1} given by Nussbaumer & Storey [8], magnetic dipole transition probabilities for $2s2p({}^3P_0 - {}^3P_1)$ and for $2s2p({}^3P_1 - {}^3P_2)$, as 5.91×10^2s^{-1} and 1.01×10^4s^{-1} respectively, and an electric quadrupole transition probability for $2s2p({}^3P_0 - {}^3P_2)$ as 7.28×10^{-1}s^{-1}, given by Bhatia and Mason [3].

We have adopted electron collision strengths calculated by Zhang & Sampson [5] for the $\Delta n = 0$ transitions with n=2, and those by Sampson, Goett, & Clark [6] for all fine-structure transitions between $n = 2$ and $n = 3$, to get the excitation rate coefficients. We have used Mewe's empirical formula [9] with modified coefficients for other n=2-4, n=3-3, and n=3-4 transitions. The Gaunt factor for collision cross section is given by Mewe's formula as $g(u) = A + Bu^{-1} + Cu^{-2} + 2Du^{-3} + E \ln u$, where $u = E/E_{ij}$, and E and E_{ij} are electron energy and the transition energy, respectively. For allowed transitions we have adopted $A = 0.075$ which is half of original value. We have used $A = 0.0375$ and $E = 0.138$ as the coefficients of Mewe's formula to match the excitation rate coefficients for $np - n's$ transitions with those by Sampson et al. Oscillator strengths are estimated from the transition probabilities when the probability is not zero. For transitions which transition probabilities are zero, we have estimated the collision strengths using oscillator strengths of other allowed lines. Here, the lower level of transition is fixed and upper level is chosen with condition in which differences of quantum numbers from the original upper level are $\Delta l = 1$, $\Delta J = 1$, and $\Delta L = 1$, or $\Delta l = -1$, $\Delta J = -1$, and $\Delta L = -1$, if such a level exists as an allowed transition. For example, for $2s2p \, {}^3P_1 - 2s3p \, {}^3P_0$ transition

the transition probability of $2s2p\ ^3P_1 - 2s3d\ ^3D_1$ transition is chosen to estimate the oscillator strength. If there is not such a transition to be borrowed in the above way, we choose a transition which has the closest transition energy with the fixed lower level. Then the oscillator strength is estimated as $f_{ij} \sim f_{ik}(borrowed)w_j/w_k$, where i and j indicate the lower and upper levels of original transition, respectively, k indicates the upper level of the borrowed transition, and f_{ik} is the oscillator strength of borrowed transition. The excitation rate coefficients calculated by Mewe's empirical formula are checked for available transitions with above data. We have included the proton collisional excitation for the three fine-structure transitions in the $2s2p\ ^3P$ levels, using the cross sections given by Doyle [10].

Zhang & Sampson calculated the collision strengths for n=2 levels with relativistic distorted-wave program. Using their data provided as a table, we have calculated the effective collision strength, γ, by approximating the integration with the Maxwellian distribution of electron velocity to a summation used orthogonal Laguerre polynomials. The formula of this approximation is given as Formula 25.4.45 in Handbook of Mathematical Functions [11]. The value of γ obtained with this method is consistent with γ calculated with fitting method described in Kato [12], where the collision strengths are fitted to the formulae which can be integrated analytically. The difference is less than 10 % at $T_e > 10^6$K. Sampson et al. used a relativistic Coulomb-Born-exchange method and gave collision strengths fitted with an analytical form for the transitions from n=2 to n=3 levels. Figure 1 shows the excitation rate coefficients for selected transitions as a function of electron temperature. For comparisons the rate coefficients calculated from data of Keenan et al. ($n = 2 - 2$ transitions) and of Bhatia and Mason ($n = 3 - 2$ transitions) are also plotted in Fig. 1.

The collision strengths used by other works [3,4] are calculated with different methods. Bhatia & Mason [3] calculated the collision strengths using distorted wave approximation for the transitions between 20 levels. Norrington & Grant [13] used a relativistic

R-matrix code to calculate the collision strengths for transitions among 10 levels, which were used by Keenan et al.[4].

3   Collisional-Radiative Model

We have calculated the level population densities and spectra by the collisional-radiative model (CRM). We have taken into account the collisional excitation between all fine-structure transitions including forbidden transitions as well as the radiative transitions;

$$\frac{dn_i}{dt} = -\sum_j (C_{ij}n_e + A_{ij})n_i + \sum_j C_{ji}n_e n_i + \sum_{j>i} A_{ji}n_i = 0, \tag{1}$$

where C_{ij} is the excitation rate coefficients from the level i to j, A_{ij} is the radiative transition probability from i to j, n_i is the population density of i level and n_e is the electron density. We assume the steady state, $dn_i/dt = 0$, to get the population density. Here, we do not take into account ionization and recombination processes from and/or to other charge states of Fe ions. The line intensity per electron and per ion from the level i to j is given as

$$\varepsilon_{ij}^{eff} = I_{ij}/n_I n_e = A_{ij}(n_i/\sum_k n_k)/n_e, \tag{2}$$

where $n_I \equiv \sum n_k$ is to normalize the population density n_i and n_e is electron density. We call ε_{ij}^{eff} the effective emission rate coefficient.

3.1   Population densities

Be-like ions have metastable state of $2s2p\ ^3P_J$. The transition probabilities from the metastable state to the ground state, $2s^2\ ^1S_0$, are quite small (§2). Since the probability $A_r(2s2p\ ^3P_0 - 2s^2\ ^1S_0)$ is zero, the population of the $2s2p\ ^3P_0$ level is not zero even at low density. Figure 2(a) shows the reduced population density relative to the population density of the ground state, $n(i)/g(i)/n(1)$, where i indicates each level, and $g(i)$ is the statistical weight of the level i, as a function of electron density at $T_e = 1.16 \times 10^7\text{K} = 1\text{keV}$. The reduced population density of $2s2p\ ^3P_0$ level is constant, 0.007,

at $n_e \lesssim 10^{12} \text{cm}^{-3}$, while densities of other levels increase proportionally to the electron density. The reduced population densities of all $n = 2$ levels become constant at $n_e \sim 10^{22} \text{cm}^{-3}$ and those of all $n = 3$ and $n = 4$ levels become constant at $n_e \sim 10^{24} \text{cm}^{-3}$, where these levels are to be populated according to the statistical weights within the same principal quantum number n.

In Fig. 2(b), the reduced population densities divided by an electron density are plotted as a function of the electron density for several levels. They indicate the density dependence of the spectral line intensities. Figure 2(b) shows that the population densities of $2p^2$ levels increase at $n_e \sim 10^{13} \text{cm}^{-3}$, according to the change of the population density of $2s2p$ $^3P_2$. Some triplet levels such as $2s3p$ ^3P_J, $2s3d$ ^3D_J, and $2s3d$ $^3D_3$, show the weak dependence similar to the $2p^2$ levels. The density effects are also seen at $10^{16} - 10^{23} \text{cm}^{-3}$. Increase of the reduced population densities of higher levels is related to the decrease of those of lower levels.

3.2   Emission line intensities

In Fig. 3 we show spectra calculated in the CRM for a plasma at an electron temperature of $1.16 \times 10^7 \text{K}$ (1keV) and electron density of 10^{11}cm^{-3}. Spectra are synthesized with Gaussian distribution with assumed instrumental resolution. The resolutions are taken as $E/\Delta E = 200$ (Fig. 3(a)) and $E/\Delta E = 500$ (Fig. 3 (b) and (c)), respectively, where ΔE is the full width of half maximum (FWHM). The unit of the spectra is the emissivity per ion and per electron (photons $\text{cm}^3\text{s}^{-1}\text{Å}^{-1}$) defined in equation (2). In UV region around 200 Å, the resonance line $(2s^2$ $^1S - 2s2p$ $^1P)$ and the inter-combination line $(2s^2$ $^1S - 2s2p$ $^3P_1)$ are much stronger compared with other lines. In X-ray region around 11 Å ($\sim$ 1keV) and 8 Å ($\sim$ 1.4keV) many lines of $n = 3 - 2$ and $n = 4 - 2$ transitions are seen. Figure 4 shows the schematic energy-level diagram of selected levels which are related to strong emission lines.

Figure 5 shows the effective emission rate coefficients defined in equation (2) for selected 17 transitions as a function of electron density at electron temperature of $1.16 \times$

10^7K. The transitions are listed in Table 3. The rate coefficients in Fig. 5 depend on the electron density similarly to the population densities shown in Fig. 2(b). Below $\sim 10^{12}$cm^{-3} there is no density dependence. The intensities of L_3, L_5, L_6, and L_{11} vary above $\sim 10^{12}$cm^{-3}. Others vary above $\sim 10^{17}$cm^{-3}. Some lines of $n = 3 - 2$ and $n = 4 - 2$ transitions show complicated variation at 10^{20-23}cm^{-3}.

Figure 6 shows the effective emission rate coefficients as a function of electron temperature at electron density of 10^{11}cm^{-3}, where there is no density effect on the line intensities. The rate coefficients of transitions among $n = 2$ levels in Fig. 6(a) are monotonic functions of the electron temperature, T_e. We find how the radiative cascades affect the line intensities at $T_e \gtrsim 10^7$K. In Fig. 6(a), thin lines represent the line intensities calculated with 10 levels, i.e. only $n = 2$ levels (case A) as Keenan et al. did. Thick lines are calculated with 46 levels, up to $n = 3$ levels (case B), and the thickest lines are calculated with 98 levels, up to $n = 4$ levels (case C). Each line is labeled with number in Table 3 and A, B, or C indicating case A, B, or C, respectively. The line intensities of case A are almost dominated by the collisional excitation from the ground state and monotonically decrease as electron temperature increases. The differences between the thin lines (case A) and the thick lines (case B and C) are prominent at $T_e \gtrsim 10^7$K, which caused by the radiative cascades from upper levels. In particular, $2p^2$ levels are fed much by the cascades and the line intensities increase as electron temperature increases. For instance, the line intensity of $2s2p\ ^1P - 2p^2\ ^1S$ transition in case A is only 10 % of that in case C at $T_e = 10^8$K. The difference between case B and C is not so large even at $T_e = 10^8$K. such as $1 \sim 14$ % different. Line intensities at $n_e = 10^{14}$cm^{-3} are also plotted with dash-dashed lines labeled such as 1' in Fig. 6(a). L_1, L_2, and L_3 are smaller than those at $n_e = 10^{11}$cm^{-3} since the population densities divided by n_e for the metastable states at $n_e = 10^{14}$cm^{-3} are smaller than that at $n_e = 10^{11}$cm^{-3} due to the collisional excitation from these levels to the upper levels. The intensities, L_5 and L_6, become larger because of the same reason.

Figure 6(b) shows the effective emission rate coefficients of $n = 3 - 2$ transitions as a function of electron temperature, T_e. In the temperature range of $3 \times 10^6 - 10^8 \mathrm{K}$, some intensities increase as temperature increases and some have a peak. Such different temperature dependences allow us to use line intensity ratios as an indicator of electron temperature. Similarly to $n = 2$ to 2 transitions, the effect of the radiative cascades is seen in the figure. The differences of case B and C become larger at higher temperature and are 1% – 28% at 10keV, depending on transitions. $2s3d$ levels are much affected by the cascades.

Figure 6(c) shows the effective emissions rate coefficients of $n = 4 - 2$ transitions. The temperature dependences are similar to $n = 3 - 2$ transitions. Note that in the calculation of population densities the excitation rate coefficients from $n = 2$ to $n = 4$ transitions are estimated by the empirical formula.

4 Line Intensity Ratios

We have chosen 17 strong lines to measure electron temperature of a plasma, which are summarized in Table 3. We take 14 pairs for line ratios summarized in Table 4. Five ratios from six lines chosen in transitions among $n = 2$ levels, are taken to be examined, as selected by Keenan et al. [4]. Six ratios from seven lines chosen among $n = 3 - 2$ transitions are taken, and three ratios from four lines chosen among $n = 4 - 2$ transitions are taken.

4.1 Density dependences

We investigate the density dependence of the above line ratios first. Figure 7 shows the line ratios listed in Table 4 as a function of electron density, n_e, at electron temperature of $1.16 \times 10^7 \mathrm{K}$. There is no density dependence seen at $n_e \lesssim 10^{12} \mathrm{cm}^{-3}$. R_6 and R_{12} are relatively insensitive to the density in the whole range, while R_2, R_3, R_5, R_9, and R_{10} vary above $n_e \sim 10^{12} \mathrm{cm}^{-3}$. Their density dependences are caused by the variation of

population densities of metastable levels. Others are almost constant at $n_e \lesssim 10^{16} \text{cm}^{-3}$.

For tokamak plasmas at electron density around $10^{13-14} \text{cm}^{-3}$ the line ratios, R_2, R_4, R_5, R_9, and R_{10}, are not good for temperature diagnostic because of strong density dependences. The ratio R_5 is found to be quite good for density diagnostic because of the small temperature dependence. Other ratios have possibilities to be used for temperature diagnostic.

4.2   Temperature dependences

Figure 8 shows the line intensity ratios as a function of electron temperature at $n_e = 10^{11} \text{cm}^{-3}$. For R_1 to R_5, we plot the ratios calculated, including 10 levels (case A), with 46 levels (case B), and with 98 levels (case C), together with the ratios obtained by Keenan et al. [4]. For R_6 to R_{10}, the ratios in cases C and B are plotted. Crosses in Fig. 8(e)-(h) are the ratios estimated from results by Bhatia and Mason [3] who calculated at an electron density of 10^9cm^{-3}. There is no density dependence for these line ratios at such density region. Bhatia and Mason obtained these ratios with 20 levels. When we calculated the ratios with the same 20 levels as theirs, the ratios are different by 1 % or less from the ratios calculated in case B (46 levels) in which $2pnl$ levels are included. So we can compare the ratios of Bhatia and Mason with ours in case B. Those ratios at $n_e = 10^{14} \text{cm}^{-3}$ in case C are also plotted in the figure.

Comparing $R_1 - R_5$ in case A with the ratios obtained by Keenan et al., we find that the differences are 1 % - 33 % and tend to increase as the electron temperature increases. R_3 and R_4 are much different. The difference is caused by the different excitation cross sections from the ground state to $2p^2$ state.

When we include $n = 3$ and 4 levels in the calculations, the line ratios are significantly changed, especially at higher temperature. It is because the cascades from upper levels contribute to the population densities and the line intensities, as seen in Fig. 6(a). For example, R_2 in case C is 93 % of R_2 in case A at $T_e = 3.5 \times 10^6 \text{K}$, 57 % at $T_e = 1.2 \times 10^7 \text{K}$, and 32 % at $T_e = 1.2 \times 10^8 \text{K}$. Similarly to the line intensities themselves, the intensity

ratios are much affected by the cascades.

The ratios R_2, R_3, and R_5 show different temperature dependences at $n_e = 10^{14} \text{cm}^{-3}$ from those at $n_e = 10^{11} \text{cm}^{-3}$, because the population densities of the metastable states depend on the density at $n_e \gtrsim 10^{12} \text{cm}^{-3}$ and the collisional excitation from the metastable states starts to affect the population densities of upper levels.

As seen in Fig. 8(e)-(h), the ratios, R_6-R_{10}, are mostly different from those obtained by Bhatia and Mason. R_7 shows good agreement with that of Bhatia and Mason within 10 % difference. In particular, R_6 and R_8 in case B are different by 17-48 % from Bhatia and Mason. Those differences are caused by difference of the excitation cross section. The collision strength of $2s^2 \, ^1S - 2s3d \, ^1D$ obtained by Sampson et al. is larger than that of Bhatia and Mason by more than factor of ten as seen in Fig. 1(b). In addition the collision strength of Sampson et al. increases monotonically as the electron energy increases, while that of Bhatia and Mason decreases at higher energy. These two effects increase the population density of $2s3d \, ^1D$ in our calculation, resulting in different value for R_6 between Bhatia and Mason and ours. For R_8, the collision strengths of $2s^2 \, ^1S - 2s3p \, ^1P$ and $2s^2 \, ^1S - 2s3p \, ^3P_1$ obtained by Sampson et al. increase similarly according to the increase of the electron energy, while the collision strength of $2s^2 \, ^1S - 2s3p \, ^1P$ obtained by Bhatia and Mason increases faster than that of $2s^2 \, ^1S - 2s3p \, ^3P$. This causes the different temperature dependences for R_8. The ratios of R_9 and R_{10} decrease slower than those of Bhatia and Mason at higher temperature.

The effect on the line ratios by including $n = 4$ levels is not large, by amount up to 25 %, for all ratios considered. We note that it is important to include levels up to $n = 3$ at least in calculations with CRM to get reliable line intensity ratios for temperature diagnostic.

As R_8 and R_{11} show small temperature dependence, a combined usage of these ratios with others is quite helpful to check the calibration of spectrometer. R_9 and R_{10} depend slightly on the electron density. R_9 at 10^{14}cm^{-3} is 1.6-2.4 times larger than that at

10^{11}cm^{-3}, and R_{10} at 10^{14}cm^{-3} is 1.2 times larger than that at 10^{11}cm^{-3}.

Although the line intensities of $n = 4 - 2$ transitions are weak, the wavelength region is not so crowded and these lines are expected to be useful for plasma diagnostics because of being unblended. R_{12} is sensitive to the electron temperature similarly to R_{11}, while R_{13} is quite insensitive to the temperature.

5 Discussion

5.1 Contribution of cascades and metastable state

We have found that the cascades are important for dominating the emission line intensity. The effect of the cascades can be examined with population densities which are calculated with following eq. (3). Only the collisional excitation from the ground state and radiative transitions are considered in the equation. Neglected excitation processes are unimportant at $n_e \lesssim 10^{15}$cm^{-3}.

$$\frac{n_i}{n_1} = \frac{C_{1i}n_e}{\sum_{j=1}^{i-1} A_{ij}} + \sum_{k=i+1}^{m} \frac{n_k}{n_1} \frac{A_{ki}}{\sum_{j=1}^{i-1} A_{ij}}, \tag{3}$$

where level 1 means the lowest level and level m means the highest level, which is 98 in this case. The first term in the right hand side is the contribution of the collisional excitation from the ground state and the second term represents the contribution of the cascades which are originated from the collisional excitation from the ground state. This equation can be calculated from the highest level for descending k. Similarly we can also examine the effect of the metastable state to the population densities separately, changing the lowest level in eq. (3) to the metastable state, $2s2p\ ^3P_0$. That is, we use C_{2i} instead of C_{1i} in eq. (3) where 2 indicate the $2s2p\ ^3P_0$ level, and we use n_2 instead of n_1. The population density of $2s2p\ ^3P_0$ itself (n_2) cannot be obtained with eq. (3), so we use the population density calculated in the CRM.

Comparing the population densities obtained with eq. (3) and those by CRM with eq. (1), we find that the cascades from $n = 3$ to $n = 2$ levels are important to the population densities of $n = 2$ levels, especially $2p^2$ state. Figure 9 shows each contribution:

the contribution of the collisional excitation from the ground state (white part in the figure); the contributions of the cascades from n=4 levels (vertical-striped part), from n=3 levels (dotted part), or from n=2 levels (horizontal-striped part); and the contribution of the metastable state (black part), for each level in the plasma at $n_e = 10^{11} \mathrm{cm}^{-3}$ and $T_e = 1.2 \times 10^7 \mathrm{K}$. Here the metastable state means $2s2p\ ^3P_0$ and the contribution from the metastable state includes both the collisional excitation from the metastable state directly to the level considered, and cascades from upper levels through the excitation from the metastable state. Considering the effect of cascades originated from the collisional excitation from the ground state, we find that the 60 % of the population density of $2p^2\ ^1S_0$ level is fed by the cascades, and 17 % of $2s2p\ ^3P_1$ level is fed by the cascades. The cascades from $n = 4$ to $n = 2$ levels contribute to the population densities by 1-10 % in $n = 2$ levels and is also effective for $2p3l$ levels and $2s3l$ triplet levels. Such percentages depend on the electron density and temperature. The above results on the radiative cascades examined with eq. (3) are consistent with the results of the differences of the line intensities in three different cases which include different number of levels in the model, discussed in §3.2. The differences between case A, B, and C mainly come from the effect of the radiative cascades.

The contribution originated from the metastable state to the population densities is mostly small, however, some triplets and $2p3l$ levels, such as $2p^2\ ^3P_1$, $2p3s\ ^3P_0$, $2p3p\ ^1P$, and $2p3d\ ^3D_2$, have population densities which originated from the metastable state by amount 50 % or more, as shown by black part in Fig. 9. The contributions of the population of the metastable state to L_2, L_3, L_5, L_6, L_{11}, and L_{12} line intensities are 6%, 10%, 4%, 2%, and 2%, respectively, at $n_e = 10^{11} \mathrm{cm}^{-3}$ and $T_e = 1.2 \times 10^7 \mathrm{K}$ (1keV). The contribution to the other lines are much less than 1%. At higher densities, the collisional excitation from excited states cannot be neglected and the eq. (3) should not be used.

5.2 Comparisons with observations of solar flares

There are some observations of FeXXIII lines emitted from the Sun. Mason et al. (1984) [14] observed a solar flare with *OSO 5* satellite and measured the intensity ratio, R_1, from the spectrum. They obtained $R_1 \simeq 23$ with ~ 25 % uncertainty. Keenan et al. discussed that their theoretical result was in good agreement with the observation of Mason et al. Our ratio, R_1, in case C is different by 4-10 % from the ratio of Keenan et al. However, it still agrees with the observation within the uncertainty, at the temperature where Be-like Fe ion (FeXXIII) has the maximum fractional abundance in ionization equilibrium ($T_e = 1.3 \times 10^7 K$, Arnaud & Rothenflug 1985 [15]). Our ratio gives a larger temperature than the ratio of Keenan et al. does. With the measurement error the electron temperature of the solar flare is obtained between $5 \times 10^6 - 6 \times 10^7 K$ in this case.

McKenzie et al. (1985) [1] observed a solar flare with *SOLEX* and showed the emission lines in the 5.5 - 12 Å range. They detected 4 lines of $n = 3 - 2$ transitions and 2 lines of $n = 4 - 2$ transitions. Since the lines at ~ 11 Å are blended and the background level is not easy to determine, their line intensities have a large uncertainty. The ratio, R_6, is measured as 2.04 with ~ 20 % uncertainty by McKenzie et al. The authors concluded that the ratio was in good agreement with one estimated by Bhatia and Mason. In our case, this ratio indicates $T_e \sim 10^{7.6\pm0.3}K$ ($2.0 \times 10^7 - 7.9 \times 10^7 K$), which is higher than the temperature, $10^{7.1\pm0.2}K$ ($7.9 \times 10^6 - 2.0 \times 10^7 K$), given by the ratio of Bhatia and Mason. On the other hand, the ratio, R_{12}, from $n = 4 - 2$ transitions is measured as 0.89 with ~ 20 % uncertainty by McKenzie et al., and this indicates $T_e \sim 10^{7.1}K$.

In future *SOHO* satellite will observe solar FeXXIII lines and will provide us more observational data to be compared with theoretical calculations.

6 Concluding Remarks

We study the spectrum of the Be-like Fe ion (FeXXIII) for plasma diagnostic and show some useful pairs of the emission lines for temperature diagnostic. In the collisional-radiative model we have included all fine structure levels up to $n = 4$ (98 levels). This is new work because previous work for plasma diagnostics includes levels of up to $2s3l$ (20 levels) [3]. We find the importance of the cascades from upper levels to the population density. However, in this study we do not take into account the effects of ionization and recombination to/from other ions.

Radiative and dielectronic recombination from Li-like Fe ion (FeXXIV) will much contribute to population densities like radiative cascades, especially at low temperature. For example, total dielectronic recombination rate coefficient is about $7 \times 10^{-12} \mathrm{cm}^3 \mathrm{s}^{-1}$ at $T_e = 1.2 \times 10^7 \mathrm{K}$ (Moribayashi et al. 1995 [16]) and the process will affect weak lines such as L_4-L_6, L_{10}-L_{17}. The recombination will increase the line intensity of L_2, $2s^2\ {}^1S - 2s2p\ {}^3P_1$, by 13 % at the maximum, where ion abundances of Li-like (FeXXIV) and Be-like (FeXXIII) ions are assumed to be equal.

Inner-sub shell ionization, $2s^2 2p + e \rightarrow 2s2p + 2e$, from B-like Fe ion (FeXXII) will make the population density of the metastable state increase, which will affect the densities of other levels (Kato et al. 1995 [17]). This inner-sub shell ionization rate coefficient can be estimated as $6.3 \times 10^{-12} \mathrm{cm}^3 \mathrm{s}^{-1}$ at $1.2 \times 10^7 \mathrm{K}$ with Lotz's formula [18]. The rate coefficient of the inner-sub shell ionization from $2s^2 2p$ to $2s2p\ {}^3P_0$ level is estimated to be proportional to the statistical weight of $2s2p$ level. When we include this effect, the population density of the level will increase by 25%, compared with that calculated only with the excitation rate coefficient from the ground state. Here, we assume that ion abundances of B-like (FeXXII) and Be-like (FeXXIII) ions are equal. The contribution to the line intensity of L_2 will be 3%. At higher temperature or with the suprathermal electrons the contribution will increase and the process will be more important. Therefore, we need to include such effects to the calculation in future work.

Acknowledgments

References

[1] McKenzie, D.L., Landecker, P.B., Feldman, U., and Doschek, G.A., Astrophys..J., **289**, 849 (1985)

[2] Fabian, A.C., Arnaud, K.A., Bautz, M.W., and Tawara, Y., Astrophys.J., **436**, L63 (1994)

[3] Bhatia, A.K. and Mason, H.E., Astron. Astrophys., **103**, 324 (1981)

[4] Keenan, F.P., Conlon, E.S., Warren, G.A., Boone, A.W., and Norrington, P.H., Astrophys.J., **405**, 350 (1993)

[5] Zhang, H.L. and Sampson, D.H., Atomic Data and Nuclear Data Tables, **52**, 143 (1992)

[6] Sampson, D.H., Goett, S.J., and Clark, R.E.H., Atomic Data and Nuclear Data Tables, **30**, 125, (1984)

[7] Dubau, J., Cornille, M., Bely-Dubau, F., Faucher, P., and Kato, T., "New Horizon of X-ray Astronomy - First Results from ASCA, Frontiers Science Series No. 12 " (Universal Academy Press, Tokyo), 615 (1994)

[8] Nussbaumer, H. and Storey, P.J., J. Phys. B., **12**, 1647, (1979)

[9] Mewe, R., Astron. Astrophys., **20**, 215 (1972)

[10] Doyle, J.G., Atomic Data and Nuclear Data Tables, **37**, 441 (1987)

[11] *HandBook of Mathematical Functions* ed. M. Abramowitz and I. A. Stegun (New York, Dover), p.890 (1965).

[12] T. Kato, Atomic Data and Nuclear Data Tables, **57**, 183 (1994)

[13] Norrington, P.H. and Grant, I.P., J. Phys. B, **20**, 4869 (1987)

[14] Mason, H.E., Bhatia, A.K., Kastner, S.O., Neupert, W.M., & Swartz, M., Sol. Phys., **92**, 199 (1984)

[15] Arnaud, M. & Rothenflug, R., Astron. Astrophys. Suppl. **60**, 425 (1985)

[16] Moribayashi, K., Kato, T., & Safronova, U., submitted to Fusion Engineering and Design (1995)

[17] Kato, T. et al. submitted to Fusion Engineering and Design (1995)

[18] Lotz, W., Astrophys.J.Suppl., **14**, 207 (1967)

Figure Captions

Fig. 1 — The excitation rate coefficients by electron collision as a function of electron temperature. (a) The rate coefficients for four $n = 2 - 2$ transitions. Solid lines are calculated with data of Zhang and Sampson [5]. Plus symbols are calculated with data of Keenan et al.[4]. (b) The rate coefficients for four $n = 2 - 3$ transitions. Solid lines are calculated with data of Sampson, Goett, & Clark [6] and dotted lines are calculated with data of Bhatia and Mason [3].

Fig. 2 — (a) The reduced population density as a function of electron density at $T_e = 1$keV for several levels.

(b) The reduced population density divided by electron density as a function of the electron density at $T_e = 1$keV for several levels of $n = 2$ and 3.

Fig. 3 — Synthesized spectra for plasma at an electron density of 10^{11}cm^3 and temperature of 1.16×10^7K (1keV). (a) Spectrum is synthesized with Gaussian distribution with spectral resolution, $R = \lambda/\Delta\lambda = 200$ for $n = 2 - 2$ transitions; (b) spectrum synthesized with $R = \lambda/\Delta\lambda = 500$ for $n = 3 - 2$ transitions; and (c) spectrum synthesized with $R = \lambda/\Delta\lambda = 500$ for $n = 4 - 2$ transitions.

Fig. 4 — Schematic energy-level diagram of selected levels for FeXXIII. Levels of $n = 3$ and 4, which are related to strong emission lines, are only drawn in the figure. Radiative transitions are labeled with the labels in Table 1.

Fig. 5 — Effective emission rate coefficients as a function of electron density at an electron temperature of 1.16×10^7K (1keV) for (a) $n = 2 - 2$ transitions, and (b) $n = 3 - 2$ and $n = 4 - 2$ transitions. Meanings of labels are listed in Table 1.

Fig. 6 — Effective emission rate coefficients as a function of electron temperature at an electron density of 10^{11}cm^{-3}. Horizontal axis is for the electron temperature measure in K (lower axis) or keV (upper axis). (a) Coefficients for transitions among $n = 2$ levels Heavy lines are calculated in case C including 98 levels up to $n = 4$, thinner lines are

in case B including 46 levels up to $n = 3$, and thinest lines are in case A including 10 levels of $n = 2$. Each line is labeled with numbers in Table 1 and A, B, or C for cases A, B, or C, respectively. 1A means L_1 lines in case A, and so on. Long dash-short dashed lines labeled with number with prime such as 1' are in case C at an electron density of 10^{14}cm^{-3}. The line 4' is overlapped with the line 4C at $n = 10^{11}\text{cm}^{-3}$; (b) For transitions from $n = 3$ to $n = 2$ levels. Heavy lines are calculated in case C and thin lines are in case B. Similarly to Fig.6a, each line is labeled with number in Table 1 ; and (c) For transitions from $n = 4$ to $n = 2$ levels. Similarly to Fig.6a, each line is labeled with number in Table 1.

Fig. 7 — The theoretical FeXXIII emission-line ratios as a function of electron density at electron temperature of $T_e = 1$ keV. Fourteen ratios from R_1 to R_{14} listed in Table 2 are plotted.

Fig. 8 — The theoretical FeXXIII emission-line ratios as a function of electron temperature at an electron density of $n_e = 10^{11}\text{cm}^{-3}$. Ratios are listed in Table 2. The label A indicates ratio calculated in case A including 10 levels of $n = 2$, B indicates case B including 46 levels up to $n = 3$, and C indicates case C including 98 levels up to $n = 4$. Ratios at $n_e = 10^{14}\text{cm}^{-3}$ in case C are also plotted with dotted lines, some of which are overlapped with lines in case C at $n = 10^{11}\text{cm}^{-3}$. Lines labeled with K in panels (a)-(d) are results by Keenan et al.[4] and crosses in panels (e)-(h) are results by Bhatia and Mason [3].

Fig. 9 — The fraction of each contribution to population density of each level at $n \leq 3$, at $T_e = 1$keV and $n_e = 10^{11}\text{cm}^{-3}$. White shows the contribution of the collisional excitation from the ground state. The contributions of cascades from $n = 2$ levels, $n = 3$ levels, and $n = 4$ levels, are shown by horizontal-striped, dotted, and vertical-striped parts, respectively. Black shows the contribution of both collisional excitation and cascades originated from the metastable state, $2s2p\ ^3P_0$.

Table 1: Energy levels (E) for FeXXIII.

Index (i)	Configuration	2s+1	L	2J	E(cm^{-1})
1	2s^2	1	0	0	0.
2	2s2p	3	1	0	339090.
3	2s2p	3	1	2	373655.
4	2s2p	3	1	4	476030.
5	2s2p	1	1	2	760531.
6	2p^2	3	1	0	943850.
7	2p^2	3	1	2	1023035.
8	2p^2	3	1	4	1073652.
9	2p^2	1	2	4	1216239.
10	2p^2	1	0	0	1436488.
11	2s3s	3	0	2	8919592.
12	2s3s	1	0	0	8991452.
13	2s3p	3	1	2	9085606.
14	2s3p	3	1	0	9085904.
15	2s3p	1	1	2	9119286.
16	2s3p	3	1	4	9123275.
17	2s3d	3	2	2	9211607.
18	2s3d	3	2	4	9216956.
19	2s3d	3	2	6	9225419.
20	2s3d	1	2	4	9288831.
21	2p3s	3	1	0	9355082.
22	2p3s	3	1	2	9373917.
23	2p3p	3	2	2	9461450.
24	2p3s	3	1	4	9488183.
25	2p3p	3	2	4	9532043.
26	2p3p	1	1	2	9533073.
27	2p3s	1	1	2	9535301.
28	2p3p	3	1	0	9554718.
29	2p3d	3	3	4	9588833.
30	2p3p	3	1	2	9630781.
31	2p3d	3	3	6	9634726.
32	2p3p	3	2	6	9638492.
33	2p3d	1	2	4	9646764.
34	2p3p	3	0	2	9655622.
35	2p3p	3	1	4	9658184.
36	2p3d	3	2	2	9665801.
37	2p3p	1	2	4	9724071.
38	2p3d	3	3	8	9733340.
39	2p3d	3	1	4	9742512.
40	2p3d	3	2	6	9768528.

Table.1 continued.

Index (i)	Configuration	2s+1	L	2J	E(cm^{-1})
41	2p3d	3	2	4	9788264.
42	2p3d	3	1	2	9788393.
43	2p3d	3	1	0	9790568.
44	2p3p	1	0	0	9802764.
45	2p3d	1	3	6	9851255.
46	2p3d	1	1	2	9861301.
47	2s4s	3	0	2	11973261.
48	2s4s	1	0	0	11996513.
49	2s4p	3	1	0	12037691.
50	2s4p	3	1	2	12039418.
51	2s4p	3	1	4	12052737.
52	2s4p	1	1	2	12057481.
53	2s4d	3	2	2	12090094.
54	2s4d	3	2	4	12091865.
55	2s4d	3	2	6	12095078.
56	2s4d	1	2	4	12114415.
57	2s4f	3	3	4	12118389.
58	2s4f	3	3	6	12119249.
59	2s4f	3	3	8	12120895.
60	2s4f	1	3	6	12125904.
61	2p4s	3	1	0	12374964.
62	2p4s	3	1	2	12379873.
63	2p4p	3	2	2	12422610.
64	2p4p	3	1	2	12449832.
65	2p4p	3	2	4	12451688.
66	2p4p	3	1	0	12453303.
67	2p4d	3	3	4	12474413.
68	2p4d	1	2	4	12491607.
69	2p4d	3	3	6	12495029.
70	2p4d	3	2	2	12499902.
71	2p4f	3	4	6	12505529.
72	2p4f	3	3	4	12508983.
73	2p4f	1	3	6	12509928.
74	2p4f	3	4	8	12510393.
75	2p4s	3	1	4	12511719.
76	2p4s	1	1	2	12519677.
77	2p4p	1	1	2	12566233.
78	2p4p	3	1	4	12572687.
79	2p4p	3	2	6	12574038.
80	2p4p	3	0	2	12578746.

Table.1 continued.

Index (i)	Configuration	2s+1	L	2J	E(cm^{-1})
81	2p4p	1	2	4	12598464.
82	2p4d	3	2	4	12613274.
83	2p4d	3	3	8	12613627.
84	2p4d	3	2	6	12621120.
85	2p4p	1	0	0	12625935.
86	2p4d	3	1	2	12628639.
87	2p4d	3	1	4	12628848.
88	2p4d	3	1	0	12629701.
89	2p4f	3	3	6	12636461.
90	2p4f	3	3	8	12639320.
91	2p4f	3	2	4	12643141.
92	2p4f	3	2	6	12643884.
93	2p4f	3	4	10	12645406.
94	2p4f	1	4	8	12647795.
95	2p4d	1	3	6	12648382.
96	2p4f	3	2	2	12650055.
97	2p4d	1	1	2	12653229.
98	2p4f	1	2	4	12654609.

Table 2: Transition probabilities (A) and the wavelengths (λ) of the transitions from i to j levels which are indices in Table 1. 5.398E+07 means 5.398×10^7.

transition i	j	A (s^{-1})	λ (Å)	transition i	j	A (s^{-1})	λ (Å)
3	1	5.398E+07	267.6264	16	7	3.236E+10	12.3453
5	1	2.003E+10	131.4870	16	8	4.105E+10	12.4229
6	3	1.183E+10	175.3787	16	9	9.272E+09	12.6470
6	5	1.814E+07	545.4983	16	11	1.472E+09	490.9577
7	2	6.654E+09	146.2105	17	2	1.297E+13	11.2708
7	3	4.139E+09	153.9930	17	3	9.414E+12	11.3148
7	4	4.210E+09	182.8136	17	4	6.179E+11	11.4474
7	5	7.801E+06	380.9465	17	5	2.095E+11	11.8328
8	3	5.511E+09	142.8578	17	13	6.237E+07	793.6464
8	4	7.108E+09	167.3298	17	14	1.397E+08	795.5270
8	5	3.819E+08	319.3656	17	15	1.658E+07	1083.1818
9	3	5.365E+08	118.6826	17	16	2.405E+06	1132.0993
9	4	5.403E+09	135.0970	18	3	1.698E+13	11.3080
9	5	4.477E+09	219.4389	18	4	5.524E+12	11.4404
10	3	1.781E+08	94.0882	18	5	1.386E+11	11.8253
10	5	3.198E+10	147.9385	18	13	1.527E+08	761.3275
11	2	3.869E+11	11.6543	18	15	2.754E+07	1023.8619
11	3	1.155E+12	11.7015	18	16	2.596E+07	1067.4604
11	4	2.029E+12	11.8433	19	4	2.206E+13	11.4294
11	5	3.236E+10	12.2563	19	16	1.385E+08	979.0169
12	3	9.210E+09	11.6039	20	3	1.150E+11	11.2168
12	5	1.309E+12	12.1493	20	4	2.273E+10	11.3471
13	1	4.673E+12	11.0064	20	5	1.586E+13	11.7257
13	6	9.242E+09	12.2824	20	13	3.419E+08	492.0644
13	7	8.600E+09	12.4030	20	15	4.176E+08	589.8127
13	8	1.042E+11	12.4813	20	16	4.279E+05	604.0244
13	9	5.687E+10	12.7075	21	7	2.508E+12	12.0019
13	10	1.034E+10	13.0734	21	11	2.279E+09	229.6265
13	11	5.086E+08	602.3577	21	17	1.478E+07	696.9864
13	12	4.253E+07	1062.0881	22	1	2.858E+11	10.6679
14	7	4.316E+10	12.4025	22	6	8.685E+11	11.8623
14	11	7.963E+08	601.2789	22	7	4.995E+11	11.9748
15	1	7.388E+12	10.9658	22	8	1.274E+12	12.0478
15	6	1.221E+10	12.2318	22	9	2.391E+08	12.2584
15	7	9.369E+08	12.3514	22	10	2.110E+10	12.5985
15	8	6.464E+10	12.4291	22	11	2.255E+09	220.1064
15	9	2.183E+11	12.6533	22	12	8.186E+08	261.4615
15	10	3.686E+09	13.0161	22	17	4.024E+06	616.1025
15	11	4.884E+08	500.7652	22	18	9.432E+06	637.0975
15	12	1.725E+08	782.2630	22	20	9.670E+05	1175.2827

Table 2. continued

| transition | | A | λ |
i	j	(s^{-1})	(Å)
23	2	9.602E+11	10.9621
23	3	2.008E+12	11.0038
23	4	6.214E+08	11.1291
23	5	1.348E+12	11.4930
23	13	2.062E+09	266.0680
23	14	6.836E+08	266.2790
23	15	1.118E+08	292.2578
23	21	7.332E+07	940.1301
23	22	7.262E+07	1142.4338
24	7	1.005E+12	11.8131
24	8	1.671E+12	11.8842
24	9	5.270E+11	12.0891
24	11	4.876E+09	175.8732
24	17	4.238E+05	361.5636
24	18	9.390E+06	368.6939
24	19	6.038E+07	380.5686
24	20	3.903E+05	501.6258
25	3	4.051E+12	10.9190
25	4	9.621E+10	11.0424
25	5	4.218E+11	11.4005
25	13	7.869E+08	223.9955
25	15	4.458E+08	242.2731
25	16	1.155E+09	244.6374
25	22	7.627E+08	632.4065
25	24	6.179E+05	2279.9681
26	2	3.192E+12	10.8767
26	3	1.039E+12	10.9177
26	4	5.904E+10	11.0411
26	5	1.413E+12	11.3992
26	13	3.167E+08	223.4801
26	14	1.816E+08	223.6289
26	15	1.453E+09	241.6702
26	16	1.627E+09	244.0227
26	21	7.301E+08	561.8241
26	22	1.425E+08	628.3150
27	1	4.560E+11	10.4873
27	6	5.884E+10	11.6395
27	7	9.074E+10	11.7478
27	8	1.113E+11	11.8180
27	9	2.102E+12	12.0206
27	10	8.202E+11	12.3475

| transition | | A | λ |
i	j	(s^{-1})	(Å)
27	11	9.425E+08	162.4143
27	12	7.988E+09	183.8745
27	17	3.496E+06	308.9333
27	18	1.684E+07	314.1240
27	20	4.679E+07	405.7294
27	23	2.377E+06	1354.0717
28	3	6.174E+12	10.8920
28	5	2.356E+11	11.3711
28	13	2.304E+09	213.1686
28	15	7.066E+08	229.6569
28	22	1.318E+09	553.0945
29	7	2.361E+11	11.6743
29	8	1.684E+12	11.7437
29	9	7.112E+11	11.9437
29	11	4.959E+06	149.4230
29	17	3.092E+08	265.0930
29	18	3.122E+08	268.9059
29	20	1.999E+08	333.3319
29	23	2.768E+08	785.0343
29	25	4.103E+06	1760.8967
29	26	8.212E+05	1793.4142
30	2	3.951E+11	10.7623
30	3	1.754E+12	10.8025
30	4	7.084E+11	10.9233
30	5	3.375E+12	11.2736
30	13	1.183E+09	183.4273
30	14	1.727E+09	183.5275
30	15	1.944E+09	195.5053
30	16	1.293E+09	197.0420
30	21	1.992E+08	362.7135
30	22	6.626E+08	389.3112
30	24	7.252E+07	701.2721
30	27	9.898E+07	1047.3383
31	8	7.098E+12	11.6808
31	9	1.538E+11	11.8786
31	18	3.934E+08	239.3659
31	19	8.058E+08	244.3151
31	20	3.411E+07	289.1055
31	25	1.743E+08	973.8759
32	4	4.319E+12	10.9141
32	16	4.739E+09	194.0929

Table 2. continued

transition		A	λ	transition		A	λ
i	j	(s^{-1})	(Å)	i	j	(s^{-1})	(Å)
32	24	6.491E+08	665.2951	36	18	2.372E+09	222.7940
33	7	1.304E+13	11.5959	36	20	2.634E+08	265.2737
33	8	1.726E+12	11.6644	36	23	3.637E+08	489.3545
33	9	1.618E+12	11.8617	36	25	1.914E+06	747.6238
33	11	1.464E+08	137.5190	36	26	3.568E+07	753.4237
33	18	1.874E+08	232.6617	36	28	1.164E+08	900.2332
33	19	1.775E+09	237.3349	36	30	6.134E+05	2855.5623
33	20	6.214E+08	279.3822	37	3	2.026E+11	10.6947
33	23	1.327E+06	539.6237	37	4	1.185E+12	10.8131
33	25	1.618E+07	871.6831	37	5	6.769E+12	11.1563
33	26	2.101E+08	879.5778	37	13	1.641E+08	156.6256
34	2	2.279E+10	10.7336	37	15	1.392E+09	165.3480
34	3	1.282E+11	10.7736	37	16	1.930E+09	166.4458
34	4	5.237E+12	10.8937	37	22	2.033E+07	285.5887
34	5	6.187E+11	11.2422	37	24	5.098E+08	423.9300
34	13	9.704E+08	175.4335	37	27	1.264E+09	529.7449
34	14	2.083E+09	175.5253	37	29	2.628E+06	739.4345
34	15	3.193E+09	186.4502	37	33	2.272E+06	1293.5416
34	16	5.924E+08	187.8473	37	36	1.292E+05	1716.1309
34	21	1.270E+07	332.7334	38	19	2.342E+09	196.8810
34	22	6.632E+07	354.9812	38	32	1.394E+08	1054.3279
34	24	8.127E+08	597.2318	39	7	1.048E+13	11.4686
34	27	2.993E+07	831.1081	39	8	2.412E+12	11.5355
35	3	2.702E+11	10.7706	39	9	2.299E+12	11.7285
35	4	4.514E+12	10.8907	39	11	2.892E+07	121.5184
35	5	2.119E+12	11.2389	39	17	1.077E+09	188.3574
35	13	3.358E+09	174.6488	39	18	4.772E+08	190.2743
35	15	3.941E+08	185.5640	39	19	1.279E+09	193.3885
35	16	1.087E+09	186.9478	39	20	1.452E+09	220.4192
35	22	3.599E+08	351.7827	39	23	3.266E+06	355.7926
35	24	7.763E+08	588.2334	39	25	1.145E+08	475.1295
35	27	7.306E+07	813.7844	39	26	3.931E+05	477.4654
36	1	1.159E+11	10.3458	39	30	1.517E+08	895.0052
36	6	2.127E+13	11.4653	39	34	1.083E+06	1150.8800
36	7	4.375E+12	11.5704	39	35	1.325E+07	1185.8365
36	8	2.274E+11	11.6385	40	8	2.224E+13	11.5010
36	9	4.087E+10	11.8349	40	9	1.966E+12	11.6928
36	10	3.035E+11	12.1517	40	18	2.182E+09	181.2999
36	11	2.696E+07	134.0107	40	19	3.122E+09	184.1250
36	12	6.619E+06	148.2912	40	20	2.231E+07	208.4652
36	17	1.037E+09	220.1703	40	25	1.360E+05	422.8610

Table 2. continued

transition		A	λ	transition		A	λ
i	j	(s^{-1})	(Å)	i	j	(s^{-1})	(Å)
40	32	9.423E+07	769.0215	43	23	1.975E+08	303.8422
40	35	1.399E+08	906.2563	43	26	1.997E+08	388.3574
40	37	5.882E+05	2249.3838	43	30	8.094E+07	625.8343
41	7	1.983E+12	11.4087	43	34	3.558E+08	741.0397
41	8	1.055E+13	11.4750	44	3	2.006E+11	10.6055
41	9	8.033E+12	11.6659	44	5	5.984E+12	11.0592
41	11	1.162E+08	115.1182	44	13	2.323E+08	139.4393
41	17	9.182E+08	173.4132	44	15	4.547E+09	146.3105
41	18	4.327E+09	175.0368	44	22	5.013E+08	233.1836
41	19	1.607E+09	177.6687	44	27	5.495E+09	373.8838
41	20	3.134E+08	200.2273	44	36	3.996E+06	730.1227
41	23	6.079E+05	305.9843	45	8	2.689E+12	11.3926
41	25	2.246E+06	390.2889	45	9	3.348E+13	11.5808
41	26	2.880E+07	391.8637	45	18	2.853E+07	157.6543
41	30	5.164E+06	634.9903	45	19	1.030E+09	159.7862
41	32	7.873E+07	667.6838	45	20	2.236E+09	177.8021
41	34	1.703E+08	753.9115	45	25	4.296E+06	313.2723
41	35	9.266E+07	768.7566	45	32	9.064E+06	470.0084
41	37	7.371E+06	1557.8088	45	35	1.378E+08	517.9446
42	1	4.272E+09	10.2162	45	37	3.124E+08	786.2661
42	6	3.318E+10	11.3064	46	1	3.642E+11	10.1406
42	7	1.181E+13	11.4085	46	6	3.675E+11	11.2140
42	8	5.450E+12	11.4748	46	7	2.540E+11	11.3144
42	9	1.733E+12	11.6657	46	8	3.429E+10	11.3796
42	10	1.658E+11	11.9733	46	9	1.095E+12	11.5673
42	11	8.400E+07	115.1012	46	10	2.041E+13	11.8697
42	12	2.858E+05	125.4798	46	11	1.752E+07	106.1898
42	17	5.391E+09	173.3745	46	12	1.191E+08	114.9624
42	18	2.118E+09	174.9974	46	17	1.102E+08	153.9184
42	20	1.765E+07	200.1756	46	18	9.162E+08	155.1961
42	23	1.051E+08	305.8638	46	20	7.024E+09	174.6816
42	25	1.474E+08	390.0929	46	23	3.127E+08	250.0927
42	26	5.033E+07	391.6661	46	25	3.791E+07	303.7132
42	28	9.443E+05	427.9458	46	26	3.447E+08	304.6660
42	30	3.687E+07	634.4716	46	28	1.531E+06	326.1758
42	34	2.552E+08	753.1804	46	30	5.842E+08	433.8014
42	35	8.227E+07	767.9964	46	34	1.302E+08	486.1944
42	37	9.851E+05	1554.6903	46	35	5.740E+06	492.3254
43	7	1.615E+13	11.4057	46	37	1.965E+07	728.7024
43	11	8.128E+07	114.8137	46	44	1.794E+07	1708.3048
43	17	7.682E+09	172.7231	47	2	9.062E+10	8.5954

Table 2. continued.

transition i	j	A (s^{-1})	λ (Å)
47	3	2.811E+11	8.6210
47	4	5.656E+11	8.6977
47	5	1.376E+10	8.9184
47	13	1.284E+11	34.6302
47	14	6.929E+10	34.6337
47	15	8.671E+10	35.0388
47	16	3.815E+11	35.0879
47	21	2.354E+08	38.1945
47	22	2.924E+08	38.4712
47	24	1.142E+09	40.2402
47	27	2.729E+08	41.0179
47	29	1.758E+07	41.9388
47	33	7.025E+08	42.9831
47	36	1.661E+08	43.3377
47	39	1.544E+08	44.8280
47	41	8.606E+08	45.7666
47	42	6.064E+08	45.7693
47	43	2.529E+08	45.8150
47	46	6.028E+07	47.3494
48	3	2.573E+09	8.6037
48	5	6.535E+11	8.9000
48	13	2.165E+11	34.3535
48	15	3.917E+11	34.7557
48	22	1.269E+10	38.1302
48	27	2.064E+10	40.6304
48	36	3.290E+08	42.9053
48	42	9.664E+06	45.2874
48	46	1.009E+09	46.8338
49	7	5.817E+05	9.0788
49	11	7.845E+11	32.0708
49	17	1.074E+11	35.3847
49	23	9.063E+07	38.8162
49	26	2.913E+09	39.9263
49	30	1.033E+09	41.5471
49	34	1.710E+09	41.9803
49	47	1.744E+08	1552.0804
50	1	9.146E+11	8.3060
50	6	1.954E+09	9.0126
50	7	6.227E+06	9.0774
50	8	4.635E+09	9.1193
50	9	9.113E+09	9.2394
50	10	2.399E+10	9.4314
50	11	6.409E+11	32.0531
50	12	1.437E+11	32.8088
50	17	2.167E+10	35.3630
50	18	7.114E+10	35.4301
50	20	2.075E+10	36.3559
50	23	3.283E+08	38.7902
50	25	1.244E+08	39.8824
50	26	2.135E+09	39.8987
50	28	3.991E+06	40.2463
50	30	2.702E+08	41.5173
50	34	1.655E+09	41.9499
50	35	4.991E+08	41.9950
50	37	1.171E+08	43.1901
50	44	1.415E+09	44.7096
50	47	1.548E+08	1511.5620
50	48	8.973E+06	2330.7601
51	7	9.119E+08	9.0664
51	8	3.315E+08	9.1082
51	11	7.654E+11	31.9168
51	17	1.028E+09	35.1973
51	18	1.523E+10	35.2636
51	19	8.844E+10	35.3692
51	20	1.301E+08	36.1807
51	23	1.781E+08	38.5909
51	25	9.356E+07	39.6716
51	26	7.950E+08	39.6878
51	30	1.302E+07	41.2889
51	32	5.788E+07	41.4208
51	34	3.423E+09	41.7168
51	35	2.645E+08	41.7614
51	37	1.245E+08	42.9430
51	47	3.266E+08	1258.2395
52	1	4.137E+12	8.2936
52	6	1.799E+10	8.9980
52	7	5.016E+06	9.0625
52	8	2.168E+10	9.1043
52	9	4.810E+10	9.2240
52	10	1.114E+11	9.4153
52	11	1.373E+11	31.8686
52	12	6.234E+11	32.6155

Table 2. continued

transition i	j	A (s^{-1})	λ (Å)	transition i	j	A (s^{-1})	λ (Å)
52	17	4.412E+09	35.1386	54	13	1.052E+12	33.2639
52	18	9.385E+09	35.2047	54	15	3.921E+11	33.6408
52	20	1.216E+11	36.1187	54	16	4.796E+11	33.6860
52	23	6.764E+05	38.5203	54	22	3.041E+08	36.7925
52	25	3.154E+08	39.5971	54	24	5.814E+07	38.4071
52	26	1.675E+08	39.6132	54	27	3.963E+08	39.1150
52	28	1.623E+09	39.9558	54	29	1.671E+08	39.9515
52	30	1.696E+08	41.2082	54	31	2.118E+09	40.6977
52	34	4.974E+08	41.6344	54	33	1.553E+09	40.8981
52	35	2.768E+08	41.6789	54	36	1.623E+09	41.2190
52	37	1.921E+09	42.8557	54	39	7.271E+07	42.5649
52	44	4.611E+09	44.3515	54	40	6.225E+08	43.0415
52	47	6.979E+07	1187.3643	54	41	1.168E+09	43.4103
52	48	1.157E+08	1640.2079	54	42	4.334E+09	43.4127
53	2	3.715E+12	8.5099	54	45	2.301E+08	44.6307
53	3	2.694E+12	8.5350	54	46	7.530E+07	44.8317
53	4	1.815E+11	8.6103	54	50	6.334E+07	1906.6705
53	5	7.263E+10	8.8265	54	51	9.568E+06	2555.7112
53	13	4.982E+11	33.2835	54	52	2.002E+06	2908.3275
53	14	1.063E+12	33.2868	55	4	6.614E+12	8.6066
53	15	3.022E+11	33.6609	55	16	1.937E+12	33.6496
53	16	5.384E+10	33.7061	55	24	3.046E+08	38.3598
53	21	5.427E+08	36.5629	55	29	2.130E+08	39.9003
53	22	7.639E+08	36.8165	55	31	2.700E+08	40.6446
53	24	4.047E+06	38.4333	55	33	4.175E+09	40.8444
53	27	2.807E+07	39.1421	55	38	2.804E+09	42.3417
53	29	3.189E+09	39.9798	55	39	8.652E+08	42.5068
53	33	9.270E+06	40.9277	55	40	2.241E+07	42.9821
53	36	8.316E+08	41.2491	55	41	4.706E+09	43.3498
53	39	7.209E+08	42.5970	55	45	8.267E+06	44.5668
53	41	5.434E+07	43.4437	55	51	4.903E+07	2361.8188
53	42	2.246E+09	43.4461	56	3	2.808E+10	8.5173
53	43	3.862E+09	43.4872	56	4	1.748E+10	8.5923
53	46	2.102E+08	44.8673	56	5	5.777E+12	8.8076
53	49	5.192E+07	1908.2700	56	13	5.132E+11	33.0163
53	50	2.874E+07	1973.3049	56	15	1.252E+12	33.3875
53	51	9.347E+05	2676.8737	56	16	4.865E+09	33.4321
53	52	1.698E+06	3066.2635	56	22	4.917E+10	36.4897
54	3	4.985E+12	8.5337	56	24	2.943E+06	38.0774
54	4	1.624E+12	8.6089	56	27	7.771E+10	38.7730
54	5	1.723E+10	8.8251	56	29	1.127E+06	39.5948

Table 2. continued.

transition		A	λ		transition		A	λ
i	j	(s⁻¹)	(Å)		i	j	(s⁻¹)	(Å)

transition i	j	A (s⁻¹)	λ (Å)
56	31	9.637E+08	40.3276
56	33	4.654E+07	40.5244
56	36	2.678E+09	40.8394
56	39	8.386E+06	42.1603
56	40	2.462E+08	42.6278
56	41	3.771E+06	42.9895
56	42	1.746E+07	42.9919
56	45	5.311E+09	44.1860
56	46	9.237E+09	44.3830
56	50	3.221E+07	1333.3873
56	51	3.759E+05	1621.3349
56	52	1.034E+08	1756.4338
57	7	1.413E+07	9.0128
57	8	1.304E+07	9.0541
57	9	2.251E+06	9.1725
57	17	3.289E+12	34.4023
57	18	6.081E+11	34.4657
57	19	1.747E+10	34.5665
57	20	2.849E+09	35.3412
57	23	3.942E+10	37.6373
57	25	5.179E+09	38.6646
57	26	5.974E+09	38.6800
57	30	2.029E+09	40.1993
57	32	9.158E+07	40.3243
57	34	5.756E+06	40.6047
57	35	4.252E+08	40.6470
57	37	1.715E+07	41.7656
57	53	7.864E+06	3534.2368
57	54	1.184E+06	3770.2256
58	8	1.792E+07	9.0534
58	9	2.919E+08	9.1718
58	18	3.462E+12	34.4555
58	19	4.231E+11	34.5563
58	20	5.025E+10	35.3305
58	25	2.206E+10	38.6517
58	32	2.225E+09	40.3103
58	35	5.094E+09	40.6328
58	37	1.711E+09	41.7506
58	54	7.511E+06	3651.8489
58	55	6.247E+05	4137.1569
59	19	3.943E+12	34.5366

transition i	j	A (s⁻¹)	λ (Å)
59	32	2.087E+10	40.2835
59	55	7.100E+06	3873.2942
60	8	4.554E+09	9.0479
60	9	1.224E+10	9.1662
60	18	3.777E+10	34.3767
60	19	1.419E+10	34.4770
60	20	3.762E+12	35.2476
60	25	2.240E+10	38.5526
60	32	7.794E+07	40.2024
60	35	1.421E+10	40.5232
60	37	3.115E+10	41.6349
60	56	6.217E+05	8704.2053
61	7	7.070E+11	8.8091
61	11	1.253E+07	28.9404
61	17	3.221E+09	31.6120
61	23	1.760E+11	34.3228
61	26	4.322E+11	35.1878
61	30	4.605E+10	36.4407
61	34	8.578E+09	36.7736
61	47	1.888E+09	248.9402
61	53	8.645E+06	351.0375
62	1	1.156E+10	8.0776
62	6	2.196E+11	8.7443
62	7	1.128E+11	8.8053
62	8	4.658E+11	8.8447
62	9	4.439E+10	8.9577
62	10	3.323E+10	9.1379
62	11	2.422E+07	28.8994
62	12	3.619E+08	29.5123
62	17	5.990E+08	31.5630
62	18	1.194E+09	31.6164
62	20	1.903E+09	32.3516
62	23	1.120E+11	34.2651
62	25	3.280E+11	35.1145
62	26	5.347E+10	35.1272
62	28	9.765E+10	35.3963
62	30	1.719E+10	36.3757
62	34	1.553E+08	36.7073
62	35	5.105E+10	36.7419
62	37	5.810E+09	37.6534
62	44	7.283E+09	38.8032

Table 2. continued

transition		A	λ	transition		A	λ
i	j	(s^{-1})	(Å)	i	j	(s^{-1})	(Å)
62	47	1.416E+09	245.9348	64	24	1.468E+08	33.7650
62	48	7.918E+08	260.8517	64	27	2.703E+10	34.3108
62	53	1.027E+06	345.0909	64	29	1.633E+09	34.9528
62	54	7.424E+06	347.2130	64	33	1.012E+11	35.6752
62	56	2.113E+07	376.7072	64	36	1.217E+10	35.9191
63	2	6.778E+11	8.2757	64	39	4.204E+09	36.9369
63	3	1.200E+12	8.2995	64	41	9.763E+08	37.5718
63	4	5.336E+07	8.3706	64	42	1.566E+09	37.5737
63	5	4.690E+11	8.5748	64	43	3.958E+09	37.6044
63	13	6.813E+09	29.9670	64	46	2.536E+09	38.6320
63	14	1.362E+08	29.9697	64	49	7.192E+06	242.6355
63	15	1.495E+10	30.2725	64	50	3.005E+06	243.6566
63	16	9.721E+07	30.3091	64	51	1.803E+09	251.8293
63	21	2.691E+11	32.5995	64	52	6.326E+08	254.8743
63	22	4.901E+11	32.8009	64	57	5.744E+05	301.7113
63	24	4.181E+08	34.0782	64	61	1.898E+08	1335.6939
63	27	2.915E+10	34.6343	64	62	7.093E+07	1429.4175
63	29	8.693E+10	35.2886	65	3	2.053E+12	8.2795
63	33	2.712E+07	36.0250	65	4	1.368E+09	8.3503
63	36	3.338E+10	36.2738	65	5	4.404E+11	8.5535
63	39	4.012E+08	37.3121	65	13	5.814E+09	29.7081
63	41	4.257E+08	37.9601	65	15	1.230E+10	30.0084
63	42	2.922E+09	37.9619	65	16	1.137E+08	30.0444
63	43	2.431E+09	37.9933	65	22	7.525E+11	32.4911
63	46	2.663E+09	39.0425	65	24	2.010E+09	33.7438
63	49	6.051E+08	259.7945	65	27	5.175E+09	34.2890
63	50	1.451E+09	260.9654	65	29	6.045E+09	34.9302
63	52	1.779E+08	273.8757	65	31	8.461E+10	35.4992
63	57	3.817E+06	328.7078	65	33	6.069E+09	35.6516
63	61	2.438E+07	2098.7966	65	36	7.277E+08	35.8952
63	62	3.309E+07	2339.8674	65	39	2.398E+09	36.9116
64	2	1.629E+12	8.2571	65	40	5.042E+09	37.2695
64	3	6.958E+11	8.2808	65	41	3.470E+08	37.5457
64	4	2.097E+09	8.3516	65	42	4.044E+09	37.5475
64	5	2.966E+11	8.5548	65	45	5.631E+09	38.4551
64	13	1.476E+09	29.7245	65	46	1.709E+09	38.6043
64	14	2.762E+08	29.7272	65	50	1.953E+08	242.5595
64	15	1.136E+10	30.0251	65	51	1.093E+09	250.6576
64	16	2.466E+08	30.0611	65	52	4.535E+08	253.6741
64	21	5.045E+11	32.3128	65	57	6.340E+05	300.0310
64	22	2.171E+11	32.5107	65	58	1.438E+05	300.8069

Table 2. continued.

transition i	j	A (s^{-1})	λ (Å)
65	60	3.466E+07	306.9515
65	62	2.534E+08	1392.4692
66	3	2.223E+12	8.2784
66	5	1.877E+11	8.5523
66	13	6.477E+09	29.6939
66	15	2.177E+10	29.9939
66	22	7.361E+11	32.4740
66	27	1.041E+08	34.2700
66	36	9.265E+10	35.8744
66	42	7.498E+08	37.5247
66	46	2.324E+09	38.5802
66	50	2.278E+09	241.6132
66	52	1.815E+05	252.6393
66	62	2.948E+08	1361.8492
67	7	6.967E+10	8.7326
67	8	7.530E+11	8.7713
67	9	1.504E+11	8.8824
67	11	3.085E+08	28.1308
67	17	1.754E+10	30.6485
67	18	1.372E+09	30.6988
67	19	3.791E+07	30.7788
67	20	2.859E+09	31.3914
67	23	1.581E+12	33.1899
67	25	2.536E+11	33.9862
67	26	3.992E+10	33.9981
67	30	1.529E+08	35.1663
67	32	8.602E+08	35.2619
67	34	6.580E+08	35.4762
67	35	3.002E+10	35.5085
67	37	1.202E+10	36.3591
67	47	5.939E+06	199.5405
67	53	6.436E+08	260.2010
67	54	5.465E+08	261.4056
67	55	1.504E+06	263.6192
67	56	3.244E+08	277.7795
67	63	7.918E+07	1930.4216
67	64	1.517E+05	4068.1741
67	65	1.152E+06	4400.4889
68	7	5.500E+12	8.7195
68	8	7.463E+11	8.7581
68	9	4.944E+10	8.8689

transition i	j	A (s^{-1})	λ (Å)
68	11	5.131E+09	27.9954
68	17	1.804E+09	30.4878
68	18	1.238E+09	30.5376
68	19	8.163E+08	30.6167
68	20	1.902E+09	31.2229
68	23	2.675E+07	33.0016
68	25	1.130E+11	33.7888
68	26	1.452E+12	33.8005
68	30	1.207E+11	34.9549
68	32	3.309E+10	35.0494
68	34	2.907E+10	35.2611
68	35	7.912E+10	35.2930
68	37	1.292E+09	36.1332
68	47	4.519E+08	192.9215
68	53	1.528E+05	249.0584
68	54	1.024E+08	250.1618
68	55	1.881E+09	252.1883
68	56	3.573E+08	265.1172
68	64	3.954E+07	2393.7772
68	65	3.023E+06	2505.0930
69	8	4.524E+12	8.7555
69	9	4.274E+11	8.8662
69	18	8.868E+09	30.5057
69	19	9.982E+06	30.5847
69	20	2.069E+10	31.1896
69	25	1.797E+12	33.7497
69	32	1.683E+09	35.0074
69	35	1.037E+11	35.2504
69	37	9.330E+09	36.0886
69	54	3.624E+08	248.0385
69	55	9.915E+08	250.0306
69	56	2.173E+08	262.7336
69	65	5.504E+07	2307.3032
70	1	8.558E+10	8.0001
70	6	6.580E+12	8.6535
70	7	1.081E+12	8.7132
70	8	1.278E+11	8.7518
70	9	2.251E+10	8.8624
70	10	4.326E+11	9.0388
70	11	2.353E+09	27.9305
70	12	5.941E+09	28.5026

Table 2. continued.

transition		A	λ	transition		A	λ
i	j	(s⁻¹)	(Å)	i	j	(s⁻¹)	(Å)
70	17	5.724E+09	30.4109	72	16	1.670E+09	29.5359
70	18	1.475E+08	30.4604	72	22	1.463E+09	31.8973
70	20	3.331E+09	31.1423	72	24	4.312E+09	33.1038
70	23	5.336E+11	32.9115	72	27	1.592E+09	33.6283
70	25	4.474E+10	33.6943	72	29	3.826E+11	34.2448
70	26	2.015E+11	33.7060	72	31	1.508E+10	34.7916
70	28	1.009E+12	33.9537	72	33	2.219E+11	34.9379
70	30	7.664E+10	34.8539	72	36	3.148E+12	35.1719
70	34	6.778E+08	35.1583	72	39	2.403E+10	36.1471
70	35	1.472E+09	35.1900	72	40	3.889E+08	36.4903
70	37	7.740E+07	36.0253	72	41	2.007E+09	36.7550
70	44	2.640E+10	37.0763	72	42	3.524E+09	36.7567
70	48	4.596E+07	198.6538	72	45	2.229E+09	37.6261
70	53	4.800E+08	244.0171	72	46	9.565E+10	37.7689
70	54	1.781E+09	245.0762	72	50	8.618E+06	212.9630
70	56	5.424E+08	259.4123	72	52	1.634E+07	221.4831
70	63	9.520E+07	1293.8096	72	57	5.079E+08	256.0202
70	64	1.256E+07	1997.2030	72	58	1.264E+09	256.5850
70	65	1.363E+06	2074.0984	72	60	3.505E+08	261.0424
70	66	3.578E+07	2145.9679	72	62	1.788E+05	774.5330
71	4	1.205E+07	8.3129	72	67	1.701E+06	2892.6455
71	16	3.674E+08	29.5661	72	68	1.149E+05	5754.8987
71	24	1.965E+09	33.1417	72	70	2.598E+05	11011.4464
71	29	3.664E+12	34.2854	73	4	7.112E+08	8.3099
71	31	2.036E+11	34.8335	73	16	1.603E+10	29.5277
71	33	5.793E+09	34.9801	73	24	4.362E+10	33.0935
71	38	2.690E+07	36.0726	73	29	3.854E+08	34.2337
71	39	1.397E+10	36.1923	73	31	1.764E+11	34.7802
71	40	1.760E+10	36.5363	73	33	3.512E+12	34.9264
71	41	1.278E+10	36.8017	73	38	5.677E+06	36.0154
71	45	2.494E+10	37.6751	73	39	1.649E+11	36.1348
71	51	2.545E+05	220.8522	73	40	3.202E+09	36.4777
71	57	8.348E+08	258.3046	73	41	5.606E+09	36.7422
71	58	6.083E+08	258.8795	73	45	2.172E+10	37.6127
71	60	2.134E+08	263.4177	73	51	1.149E+07	218.7272
71	67	1.199E+07	3213.7659	73	57	7.476E+05	255.4026
72	3	2.461E+09	8.2404	73	58	1.414E+08	255.9646
72	4	2.887E+08	8.3105	73	59	1.623E+09	257.0480
72	5	3.754E+05	8.5118	73	60	3.686E+08	260.4003
72	13	1.401E+10	29.2109	73	68	2.202E+06	5458.1786
72	15	2.061E+09	29.5012	74	31	3.399E+12	34.7745

Table 2. continued.

| transition | | A | λ | transition | | A | λ |
i	j	(s⁻¹)	(Å)	i	j	(s⁻¹)	(Å)
74	38	8.488E+08	36.0094	76	20	1.879E+09	30.9516
74	40	2.478E+11	36.4715	76	23	1.355E+09	32.6987
74	45	2.037E+11	37.6062	76	25	1.767E+10	33.4713
74	58	2.154E+08	255.6603	76	26	1.309E+10	33.4828
74	59	8.641E+08	256.7411	76	28	2.395E+09	33.7273
74	60	7.991E+08	260.0853	76	30	1.592E+11	34.6153
74	69	1.498E+06	6508.5982	76	34	1.427E+10	34.9155
75	7	1.823E+11	8.7042	76	35	3.666E+10	34.9468
75	8	9.570E+10	8.7427	76	37	3.278E+11	35.7704
75	9	3.413E+11	8.8531	76	44	1.207E+11	36.8065
75	11	4.875E+08	27.8387	76	47	1.332E+09	183.0107
75	17	1.771E+08	30.3020	76	48	4.211E+09	191.1447
75	18	7.118E+08	30.3512	76	53	4.908E+06	232.7839
75	19	1.500E+09	30.4293	76	54	3.750E+06	233.7476
75	20	3.170E+08	31.0281	76	56	1.001E+08	246.7537
75	23	1.687E+09	32.7840	76	63	1.412E+06	1030.2193
75	25	4.833E+10	33.5607	76	64	1.404E+06	1431.7292
75	26	1.835E+11	33.5723	76	65	8.126E+05	1470.8196
75	30	1.408E+09	34.7109	76	66	1.492E+05	1506.6003
75	32	2.478E+11	34.8041	77	2	9.184E+09	8.1785
75	34	6.599E+10	35.0128	77	3	3.614E+11	8.2017
75	35	1.385E+11	35.0442	77	4	7.088E+11	8.2712
75	37	8.522E+10	35.8725	77	5	1.628E+12	8.4705
75	47	4.006E+09	185.7154	77	13	4.226E+09	28.7305
75	53	3.270E+06	237.1775	77	14	1.051E+07	28.7329
75	54	3.091E+07	238.1779	77	15	8.346E+09	29.0112
75	55	1.352E+08	240.0142	77	16	6.873E+07	29.0448
75	56	7.581E+07	251.6960	77	21	1.367E+09	31.1415
75	63	2.120E+05	1122.2207	77	22	3.745E+10	31.3252
75	64	1.585E+07	1615.8241	77	24	2.233E+11	32.4881
75	65	3.653E+06	1665.7887	77	27	5.268E+11	32.9932
76	1	9.856E+09	7.9874	77	29	1.006E+08	33.5863
76	6	1.357E+10	8.6387	77	33	8.446E+09	34.2528
76	7	5.356E+10	8.6982	77	36	4.188E+09	34.4776
76	8	1.452E+10	8.7367	77	39	5.825E+10	35.4143
76	9	7.645E+11	8.8469	77	41	2.792E+09	35.9975
76	10	3.288E+11	9.0227	77	42	7.871E+09	35.9992
76	11	1.440E+06	27.7771	77	43	8.544E+09	36.0274
76	12	1.205E+08	28.3429	77	46	3.424E+10	36.9695
76	17	4.934E+07	30.2291	77	49	2.280E+09	189.1996
76	18	2.756E+08	30.2781	77	50	9.717E+08	189.8198

Table 2. continued.

transition		A	λ	transition		A	λ
i	j	(s⁻¹)	(Å)	i	j	(s⁻¹)	(Å)
77	51	3.351E+08	194.7435	79	16	2.054E+07	28.9791
77	52	2.078E+09	196.5595	79	24	7.702E+11	32.4059
77	57	1.798E+06	223.2919	79	29	2.892E+08	33.4985
77	61	1.143E+07	522.8237	79	31	9.949E+07	34.0216
77	62	5.533E+07	536.5953	79	33	4.451E+09	34.1615
77	67	5.027E+05	1089.0805	79	38	7.622E+10	35.2026
77	68	1.032E+07	1340.0040	79	39	2.271E+08	35.3167
77	70	1.443E+06	1507.5771	79	40	2.051E+10	35.6441
77	75	2.868E+07	1834.4013	79	41	2.279E+10	35.8967
77	76	4.589E+07	2147.9501	79	45	4.667E+08	36.7271
78	3	1.632E+10	8.1974	79	51	4.496E+09	191.8280
78	4	1.802E+12	8.2667	79	57	1.163E+05	219.4674
78	5	7.264E+11	8.4659	79	58	1.667E+06	219.8823
78	13	1.270E+09	28.6773	79	59	4.359E+06	220.6813
78	15	4.216E+09	28.9570	79	60	9.242E+05	223.1475
78	16	1.860E+07	28.9905	79	67	9.558E+05	1003.7651
78	22	1.530E+08	31.2620	79	68	3.461E+07	1213.1362
78	24	5.861E+11	32.4201	79	69	3.764E+05	1265.6784
78	27	1.964E+11	32.9230	79	75	1.456E+08	1604.6720
78	29	2.174E+07	33.5137	80	2	9.139E+08	8.1702
78	31	3.158E+09	34.0372	80	3	1.837E+11	8.1933
78	33	4.003E+09	34.1773	80	4	1.910E+12	8.2626
78	36	2.193E+09	34.4011	80	5	6.750E+11	8.4615
78	39	1.403E+10	35.3335	80	13	3.846E+09	28.6275
78	40	5.396E+10	35.6613	80	14	1.986E+08	28.6300
78	41	6.700E+09	35.9141	80	15	1.780E+09	28.9062
78	42	1.713E+10	35.9157	80	16	1.505E+09	28.9396
78	45	1.755E+10	36.7454	80	21	2.873E+07	31.0206
78	46	1.015E+09	36.8815	80	22	1.145E+10	31.2029
78	50	4.156E+09	187.5226	80	24	5.183E+11	32.3566
78	51	3.049E+08	192.3263	80	27	2.004E+11	32.8575
78	52	1.133E+07	194.0973	80	29	1.677E+08	33.4458
78	57	4.640E+06	220.1198	80	33	3.192E+09	34.1066
78	58	1.751E+06	220.5372	80	36	8.317E+08	34.3295
78	60	3.359E+07	223.8221	80	39	1.197E+10	35.2580
78	62	3.248E+07	518.6348	80	41	7.768E+10	35.8361
78	67	1.811E+06	1017.5600	80	42	4.808E+10	35.8378
78	68	3.508E+07	1233.3441	80	43	1.708E+10	35.8657
78	75	1.039E+08	1640.2201	80	46	1.964E+10	36.7993
78	76	2.424E+07	1886.4456	80	49	1.134E+09	184.8239
79	4	2.240E+12	8.2658	80	50	1.115E+09	185.4157

Table 2. continued.

transition		A	λ	transition		A	λ
i	j	(s⁻¹)	(Å)	i	j	(s⁻¹)	(Å)
80	51	8.480E+08	190.1108	82	8	9.698E+11	8.6658
80	52	2.938E+09	191.8410	82	9	8.223E+11	8.7742
80	61	1.205E+05	490.7198	82	11	2.438E+08	27.0733
80	62	1.838E+07	502.8324	82	17	8.480E+08	29.3974
80	67	4.174E+05	958.4623	82	18	2.199E+09	29.4436
80	68	3.188E+07	1147.5805	82	19	2.161E+07	29.5172
80	70	5.088E+05	1268.3142	82	20	2.563E+09	30.0802
80	75	1.191E+08	1491.9380	82	23	5.307E+09	31.7277
80	76	3.380E+07	1692.9288	82	25	9.045E+10	32.4546
81	3	2.126E+11	8.1801	82	26	7.038E+10	32.4654
81	4	6.331E+11	8.2492	82	30	1.260E+12	33.5290
81	5	2.025E+12	8.4474	82	32	1.614E+10	33.6159
81	13	4.616E+09	28.4668	82	34	1.577E+10	33.8106
81	15	9.529E+09	28.7424	82	35	3.213E+11	33.8399
81	16	5.169E+07	28.7754	82	37	1.623E+11	34.6116
81	22	1.105E+10	31.0121	82	47	6.922E+05	156.2469
81	24	1.827E+11	32.1514	82	53	1.341E+09	191.1390
81	27	5.625E+11	32.6460	82	54	2.824E+08	191.7883
81	29	1.229E+09	33.2267	82	55	5.908E+08	192.9771
81	31	1.272E+09	33.7412	82	56	2.491E+09	200.4575
81	33	4.763E+09	33.8788	82	63	8.777E+05	524.4850
81	36	1.680E+09	34.0987	82	64	1.350E+05	611.8374
81	39	4.756E+07	35.0146	82	65	2.400E+07	618.8662
81	40	7.155E+09	35.3365	82	71	7.359E+05	928.1180
81	41	8.012E+09	35.5847	82	72	2.030E+06	958.8589
81	42	1.690E+08	35.5863	82	73	8.326E+05	967.6233
81	45	9.440E+10	36.4006	82	77	4.393E+07	2125.8282
81	46	1.362E+10	36.5342	82	78	9.637E+06	2463.8576
81	50	1.762E+07	178.8760	82	79	1.778E+05	2548.6696
81	51	2.113E+09	183.2418	82	80	1.903E+06	2896.2611
81	52	1.765E+09	184.8487	82	81	1.131E+05	6752.4328
81	57	6.748E+06	208.3007	83	19	8.835E+09	29.5141
81	60	1.412E+08	211.6130	83	32	1.941E+12	33.6119
81	62	4.800E+06	457.4749	83	55	3.641E+09	192.8456
81	67	5.587E+05	806.1163	83	73	2.573E+05	964.3251
81	68	1.124E+07	935.8244	83	79	4.234E+07	2525.9142
81	69	1.040E+06	966.7843	84	8	5.864E+12	8.6599
81	70	2.438E+05	1014.5835	84	9	3.629E+11	8.7682
81	75	1.149E+08	1152.8080	84	18	2.616E+09	29.3758
81	76	2.567E+08	1269.2445	84	19	2.205E+09	29.4490
82	7	2.108E+12	8.6280	84	20	2.077E+09	30.0094

Table 2. continued.

transition		A	λ		transition		A	λ
i	j	(s⁻¹)	(Å)		i	j	(s⁻¹)	(Å)
84	25	5.315E+10	32.3721		86	25	2.441E+10	32.2935
84	32	6.208E+11	33.5275		86	26	4.078E+10	32.3043
84	35	1.207E+12	33.7503		86	28	6.574E+07	32.5317
84	37	4.505E+10	34.5179		86	30	2.157E+11	33.3572
84	54	3.021E+09	188.9449		86	34	1.167E+12	33.6359
84	55	1.564E+09	190.0986		86	35	3.686E+11	33.6649
84	56	2.674E+07	197.3534		86	37	7.119E+10	34.4285
84	65	1.315E+05	590.2062		86	44	1.546E+10	35.3873
84	71	3.692E+05	865.1161		86	53	4.732E+09	185.6856
84	72	2.552E+05	891.7652		86	54	1.618E+09	186.2982
84	73	1.149E+05	899.3411		86	56	2.263E+07	194.4677
84	74	5.914E+06	903.1189		86	63	1.138E+07	485.3695
84	78	4.931E+07	2064.6964		86	64	6.097E+06	559.2607
84	79	2.148E+07	2123.9240		86	65	1.847E+07	565.1276
84	81	3.338E+05	4413.8445		86	77	3.834E+07	1602.4135
85	3	2.666E+11	8.1617		86	78	2.718E+07	1787.2419
85	5	1.917E+12	8.4279		86	80	4.248E+07	2004.3033
85	13	1.467E+10	28.2460		86	81	5.882E+05	3314.0179
85	15	2.539E+10	28.5173		87	7	7.901E+11	8.6164
85	22	1.028E+10	30.7501		87	8	3.155E+12	8.6541
85	27	6.328E+11	32.3558		87	9	2.788E+12	8.7622
85	36	4.662E+06	33.7822		87	11	5.078E+09	26.9596
85	42	3.580E+09	35.2418		87	17	2.420E+07	29.2634
85	46	1.096E+11	36.1712		87	18	7.709E+05	29.3092
85	50	1.515E+07	170.4979		87	19	4.503E+09	29.3821
85	52	5.428E+09	175.9158		87	20	2.334E+08	29.9400
85	62	1.378E+08	406.4013		87	23	9.570E+07	31.5717
85	70	1.280E+06	793.4392		87	25	1.541E+10	32.2914
85	76	9.302E+08	941.1054		87	26	5.210E+08	32.3021
86	1	2.288E+09	7.9185		87	30	2.087E+10	33.3548
86	6	1.034E+09	8.5581		87	32	1.205E+11	33.4408
86	7	4.082E+12	8.6165		87	34	7.740E+11	33.6335
86	8	1.750E+12	8.6543		87	35	5.834E+11	33.6625
86	9	5.316E+11	8.7624		87	37	4.058E+11	34.4261
86	10	9.409E+10	8.9348		87	47	3.333E+06	152.5351
86	11	7.246E+09	26.9611		87	53	8.453E+08	185.6136
86	12	1.607E+08	27.4938		87	54	3.338E+09	186.2258
86	17	2.616E+08	29.2652		87	55	1.236E+09	187.3465
86	18	5.896E+09	29.3110		87	56	6.146E+08	194.3888
86	20	1.011E+08	29.9418		87	63	1.539E+05	484.8783
86	23	2.029E+07	31.5737		87	64	2.793E+06	558.6086

Table 2. continued.

| transition | | A | λ |
i	j	(s⁻¹)	(Å)
87	65	1.620E+06	564.4618
87	71	4.746E+05	810.9049
87	77	4.691E+05	1597.0716
87	78	2.744E+07	1780.5991
87	79	1.172E+07	1824.4757
87	80	3.768E+07	1995.9528
87	81	4.326E+06	3291.2505
88	7	5.263E+12	8.6157
88	11	1.015E+10	26.9534
88	17	7.914E+09	29.2561
88	23	3.096E+08	31.5632
88	26	3.529E+10	32.2932
88	30	1.976E+11	33.3453
88	34	1.663E+12	33.6239
88	47	1.873E+06	152.3369
88	53	6.707E+09	185.3201
88	63	2.949E+07	482.8804
88	64	2.313E+07	555.9586
88	77	5.252E+07	1575.5998
88	80	6.400E+07	1962.5283
89	16	1.881E+07	28.4642
89	24	1.353E+08	31.7634
89	29	1.369E+10	32.8124
89	31	9.970E+10	33.3141
89	33	1.389E+11	33.4482
89	38	2.244E+10	34.4457
89	39	2.836E+12	34.5549
89	40	4.891E+11	34.8683
89	41	1.992E+11	35.1099
89	45	1.472E+11	35.9040
89	57	1.872E+09	193.0234
89	58	1.098E+09	193.3442
89	59	6.972E+07	193.9617
89	60	1.195E+09	195.8644
89	67	3.026E+06	617.0998
89	68	2.829E+06	690.3483
89	69	4.366E+06	707.0513
89	75	2.047E+05	801.6580
89	82	4.023E+06	4312.7091
89	84	2.241E+05	6518.5765
90	31	1.133E+11	33.2824
90	38	6.656E+11	34.4118
90	40	2.861E+12	34.8336
90	45	2.749E+11	35.8672
90	58	2.215E+09	192.2814
90	59	1.928E+09	192.8921
90	60	2.886E+08	194.7737
90	69	5.643E+06	693.0421
90	83	1.157E+06	3892.1487
90	84	1.861E+06	5494.5930
91	3	2.719E+06	8.1503
91	4	7.413E+07	8.2189
91	5	1.186E+10	8.4157
91	13	9.304E+09	28.1093
91	15	2.208E+06	28.3780
91	16	2.066E+09	28.4102
91	22	3.680E+09	30.5883
91	24	3.037E+09	31.6961
91	27	6.994E+09	32.1767
91	29	1.710E+09	32.7406
91	31	7.561E+09	33.2401
91	33	1.396E+10	33.3736
91	36	2.237E+10	33.5870
91	39	5.283E+11	34.4753
91	40	1.247E+11	34.7873
91	41	8.414E+11	35.0278
91	42	1.852E+12	35.0294
91	45	4.206E+07	35.8181
91	46	5.106E+11	35.9474
91	50	5.595E+07	165.6388
91	51	1.311E+07	169.3756
91	52	2.585E+07	170.7476
91	57	3.531E+09	190.5661
91	58	1.013E+09	190.8789
91	60	5.450E+08	193.3347
91	62	1.159E+06	379.8409
91	67	6.004E+05	592.6680
91	68	1.126E+06	659.9153
91	69	3.589E+05	675.1619
91	76	3.579E+06	809.9530
91	82	1.722E+06	3348.1257
91	84	1.316E+05	4541.1306

Table 2. continued.

| transition | | A | λ | transition | | A | λ |
i	j	(s^{-1})	(Å)	i	j	(s^{-1})	(Å)
91	86	6.341E+05	6895.5618	95	20	2.850E+10	29.7659
91	87	2.458E+05	6996.2625	95	25	4.078E+10	32.0889
92	4	6.600E+07	8.2184	95	32	3.064E+10	33.2238
92	16	1.109E+10	28.4042	95	35	9.739E+10	33.4426
92	24	1.791E+10	31.6887	95	37	1.710E+12	34.1961
92	29	6.517E+09	32.7327	95	54	8.936E+07	179.6890
92	31	3.361E+08	33.2319	95	55	1.443E+09	180.7322
92	33	3.800E+10	33.3654	95	56	2.087E+09	187.2773
92	38	3.670E+10	34.3578	95	65	4.337E+06	508.4028
92	39	3.962E+11	34.4665	95	71	1.681E+06	700.0177
92	40	6.401E+11	34.7783	95	72	2.567E+06	717.3640
92	41	2.535E+12	35.0187	95	73	2.022E+06	722.2583
92	45	2.670E+11	35.8086	95	74	7.946E+06	724.6928
92	51	3.932E+07	169.1628	95	78	3.323E+07	1321.0846
92	57	1.313E+08	190.2968	95	79	3.737E+06	1345.0844
92	58	1.710E+09	190.6087	95	81	7.262E+07	2003.2815
92	59	1.677E+09	191.2088	96	2	7.449E+07	8.1228
92	60	1.523E+09	193.0576	96	3	2.171E+07	8.1457
92	67	2.175E+05	590.0710	96	5	3.140E+07	8.4108
92	68	1.690E+06	656.6971	96	13	5.511E+09	28.0548
92	69	9.228E+05	671.7936	96	14	1.120E+10	28.0572
92	75	3.544E+06	756.6342	96	15	3.021E+09	28.3224
92	82	1.200E+06	3266.8984	96	16	6.059E+08	28.3545
92	84	7.324E+05	4392.9851	96	21	1.028E+10	30.3493
92	87	9.361E+05	6650.7214	96	22	7.132E+09	30.5237
93	38	3.926E+12	34.3399	96	24	9.092E+08	31.6268
93	59	4.293E+09	190.6539	96	27	3.179E+09	32.1053
93	83	1.374E+07	3146.7587	96	29	2.037E+09	32.6667
94	31	3.711E+11	33.1888	96	33	3.428E+07	33.2968
94	38	9.235E+09	34.3117	96	36	7.988E+09	33.5092
94	40	1.651E+11	34.7311	96	39	3.517E+10	34.3933
94	45	3.219E+12	35.7585	96	41	2.308E+11	34.9432
94	58	1.522E+09	189.1982	96	42	1.818E+12	34.9447
94	59	5.862E+08	189.7895	96	43	1.820E+12	34.9713
94	60	2.924E+09	191.6108	96	46	1.013E+10	35.8583
94	69	2.147E+07	654.5945	96	49	3.515E+07	163.3015
94	84	8.160E+05	3748.8758	96	50	1.949E+07	163.7634
95	8	2.618E+11	8.6395	96	51	1.376E+06	167.4151
95	9	1.147E+13	8.7473	96	52	5.582E+06	168.7554
95	18	1.715E+09	29.1424	96	57	5.900E+09	188.0880
95	19	5.415E+07	29.2144	96	61	8.426E+06	363.5162

Table 2. continued.

transition i	j	A (s^{-1})	λ (Å)
96	62	4.437E+06	370.1208
96	67	3.399E+05	569.3385
96	70	3.923E+05	665.9853
96	75	2.557E+05	722.8799
96	76	1.015E+06	767.0013
96	82	1.751E+05	2718.7677
96	86	1.923E+06	4669.4071
96	87	2.378E+05	4715.3664
96	88	1.650E+06	4913.0478
97	1	1.538E+11	7.9031
97	6	4.382E+11	8.5402
97	7	1.223E+11	8.5983
97	8	2.034E+09	8.6359
97	9	4.296E+11	8.7436
97	10	6.591E+12	8.9152
97	11	9.736E+08	26.7835
97	12	9.946E+09	27.3091
97	17	5.282E+08	29.0561
97	18	1.297E+08	29.1013
97	20	9.665E+09	29.7230
97	23	1.714E+10	31.3305
97	25	1.724E+09	32.0391
97	26	6.653E+10	32.0497
97	28	3.033E+10	32.2736
97	30	5.425E+11	33.0858
97	34	1.935E+11	33.3599
97	35	5.097E+07	33.3885
97	37	4.206E+10	34.1395
97	44	1.006E+12	35.0820
97	47	7.095E+05	147.0657
97	48	1.714E+08	152.2729
97	53	1.102E+08	177.5773
97	54	1.035E+09	178.1376
97	56	6.088E+09	185.5927
97	63	4.246E+07	433.6161
97	64	3.771E+07	491.6478
97	65	7.947E+06	496.1762
97	66	3.764E+06	500.1835
97	72	4.539E+06	693.2594
97	77	1.187E+08	1149.4781
97	78	4.155E+05	1241.5840
97	80	5.493E+07	1342.5920
97	81	4.414E+06	1825.9840
97	85	6.957E+06	3663.8088
98	3	5.163E+07	8.1427
98	4	1.732E+08	8.2111
98	5	2.530E+10	8.4075
98	13	1.309E+06	28.0190
98	15	1.742E+10	28.2860
98	16	2.276E+09	28.3179
98	22	8.399E+09	30.4814
98	24	3.745E+09	31.5813
98	27	4.286E+06	32.0584
98	29	4.141E+09	32.6182
98	31	8.160E+07	33.1139
98	33	4.402E+10	33.2464
98	36	8.483E+10	33.4581
98	39	1.889E+11	34.3395
98	40	2.843E+10	34.6491
98	41	6.082E+11	34.8876
98	42	3.244E+11	34.8892
98	45	1.650E+10	35.6715
98	46	2.580E+12	35.7998
98	50	2.511E+06	162.5510
98	51	6.788E+05	166.1483
98	52	1.770E+08	167.4683
98	57	6.483E+07	186.4905
98	58	1.666E+09	186.7900
98	60	3.808E+09	189.1411
98	62	9.088E+06	363.9854
98	67	1.324E+06	554.9492
98	68	1.239E+06	613.4866
98	69	2.149E+05	626.6419
98	70	5.522E+06	646.3802
98	75	3.484E+06	699.8400
98	76	7.033E+05	741.1134
98	82	1.774E+06	2419.2211
98	84	1.174E+05	2986.0453
98	86	4.617E+05	3850.5607
98	87	1.254E+06	3881.7603

Table 3: Strong Emission Lines of FeXXIII Ions

label		transitions	wavelength (in Å)	(in eV)
L_1	$\cdots$	$2s^2\ {}^1S - 2s2p\ {}^1P$	131.48 Å	94.296eV
L_2	$\cdots$	$2s^2\ {}^1S - 2s2p\ {}^3P_1$	267.62 Å	46.328eV
L_3	$\cdots$	$2s2p\ {}^3P_1 - 2s2p\ {}^3P_2$	976.78 Å	12.693eV
L_4	$\cdots$	$2s2p\ {}^1P - 2p^2\ {}^1S$	146.21 Å	84.800eV
L_5	$\cdots$	$2s2p\ {}^1P - 2p^2\ {}^1D$	219.43 Å	56.502eV
L_6	$\cdots$	$2s2p\ {}^3P_2 - 2p^2\ {}^3P_2$	167.33 Å	74.097eV
L_7	$\cdots$	$2s2p\ {}^1P - 2s3d\ {}^1D$	11.725 Å	1057.4 eV
L_8	$\cdots$	$2s2p\ {}^1P - 2s3s\ {}^1S$	12.149 Å	1020.5 eV
L_9	$\cdots$	$2s^2\ {}^1S - 2s3p\ {}^1P$	10.966 Å	1130.7 eV
L_{10}	$\cdots$	$2s^2\ {}^1S - 2s3p\ {}^3P_1$	11.006 Å	1126.5 eV
L_{11}	$\cdots$	$2s2p\ {}^3P_2 - 2s3d\ {}^3D_3$	11.429 Å	1084.8 eV
L_{12}	$\cdots$	$2s2p\ {}^3P_1 - 2s3d\ {}^3D_2$	11.308 Å	1130.8 eV
L_{13}	$\cdots$	$2p^2\ {}^1S - 2p3d\ {}^1P$	11.869 Å	1044.6 eV
L_{14}	$\cdots$	$2s2p\ {}^1P - 2s4d\ {}^1D$	8.8074 Å	1407.7 eV
L_{15}	$\cdots$	$2s^2\ {}^1S - 2s4p\ {}^1P$	8.2934 Å	1495.0 eV
L_{16}	$\cdots$	$2s2p\ {}^1P - 2s4s\ {}^1S$	8.8998 Å	1393.1 eV
L_{17}	$\cdots$	$2s^2\ {}^1S - 2s4p\ {}^3P_1$	8.3059 Å	1492.7 eV

Table 4: Emission Lines Ratios for Plasma Diagnostics

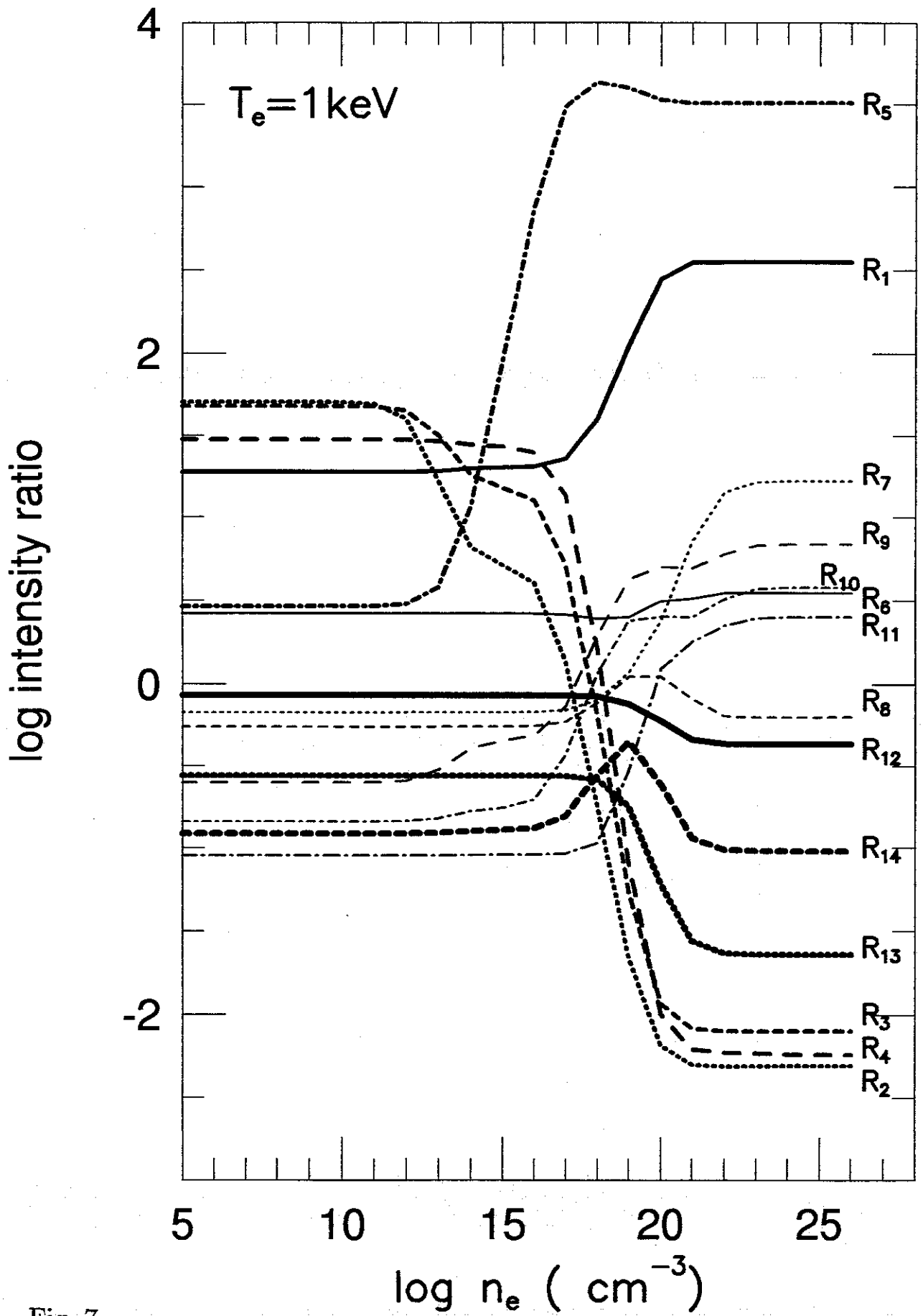| label	ratios	with labels in Table 1
R_1	$\cdots$ $I(2s^2\,^1S - 2s2p\,^1P)/I(2s^2\,^1S - 2s2p\,^3P_1)$	L_1/L_2
R_2	$\cdots$ $I(2s^2\,^1S - 2s2p\,^3P_1)/I(2s2p\,^3P_2 - 2p^2\,^3P_2)$	L_2/L_6
R_3	$\cdots$ $I(2s^2\,^1S - 2s2p\,^3P_1)/I(2s2p\,^1P - 2p^2\,^1D)$	L_2/L_5
R_4	$\cdots$ $I(2s^2\,^1S - 2s2p\,^3P_1)/I(2s2p\,^1P - 2p^2\,^1S)$	L_2/L_4
R_5	$\cdots$ $I(2s^2\,^1S - 2s2p\,^3P_1)/I(2s2p\,^3P_1 - 2s2p\,^3P_2)$	L_2/L_3
R_6	$\cdots$ $I(2s2p\,^1P - 2s3d\,^1D)/I(2s^2\,^1S - 2s3p\,^1P)$	L_7/L_9
R_7	$\cdots$ $I(2s^2\,^1S - 2s3p\,^1P)/I(2s2p\,^1P - 2s3s\,^1S)$	L_9/L_8
R_8	$\cdots$ $I(2s^2\,^1S - 2s3p\,^3P_1)/I(2s^2\,^1S - 2s3p\,^1P)$	L_{10}/L_9
R_9	$\cdots$ $I(2s2p\,^3P_2 - 2s3d\,^3D_3)/I(2s^2\,^1S - 2s3p\,^1P)$	L_{11}/L_9
R_{10}	$\cdots$ $I(2s2p\,^3P_1 - 2s3d\,^3D_2)/I(2s^2\,^1S - 2s3p\,^1P)$	L_{12}/L_9
R_{11}	$\cdots$ $I(2p^2\,^1S - 2p3d\,^1P)/I(2s^2\,^1S - 2s3p\,^1P)$	L_{13}/L_9
R_{12}	$\cdots$ $I(2s^2\,^1S - 2s4p\,^1P)/I(2s2p\,^1P - 2s4d\,^1D)$	L_{14}/L_{13}
R_{13}	$\cdots$ $I(2s2p\,^1P - 2s4s\,^1S)/I(2s2p\,^1P - 2s4d\,^1D)$	L_{15}/L_{13}
R_{14}	$\cdots$ $I(2s^2\,^1S - 2s4p\,^3P_1)/I(2s2p\,^1P - 2s4d\,^1D)$	L_{16}/L_{13}
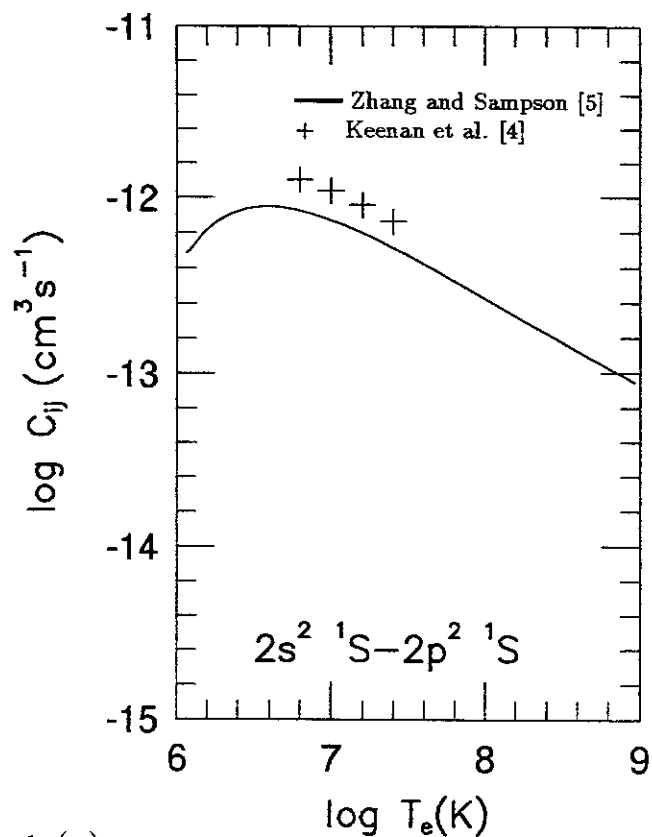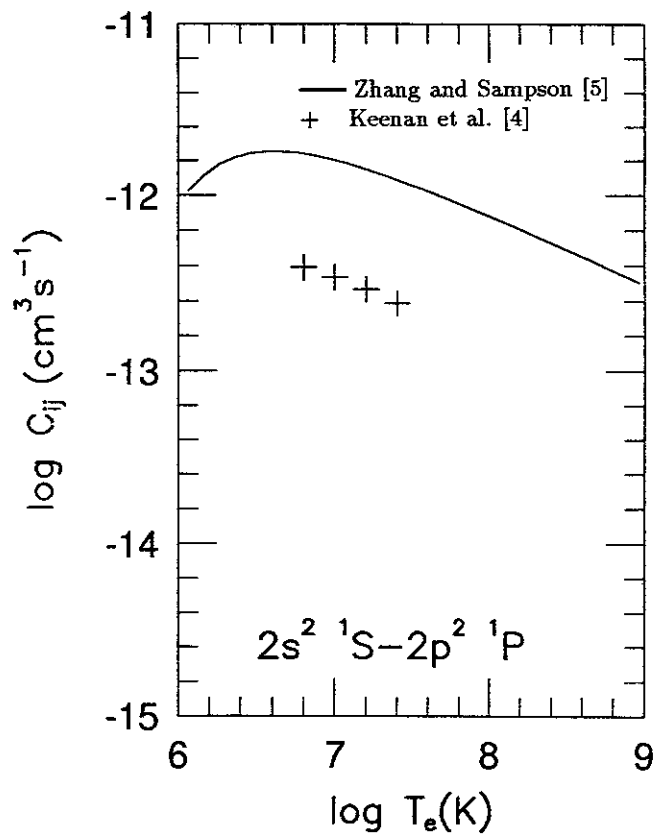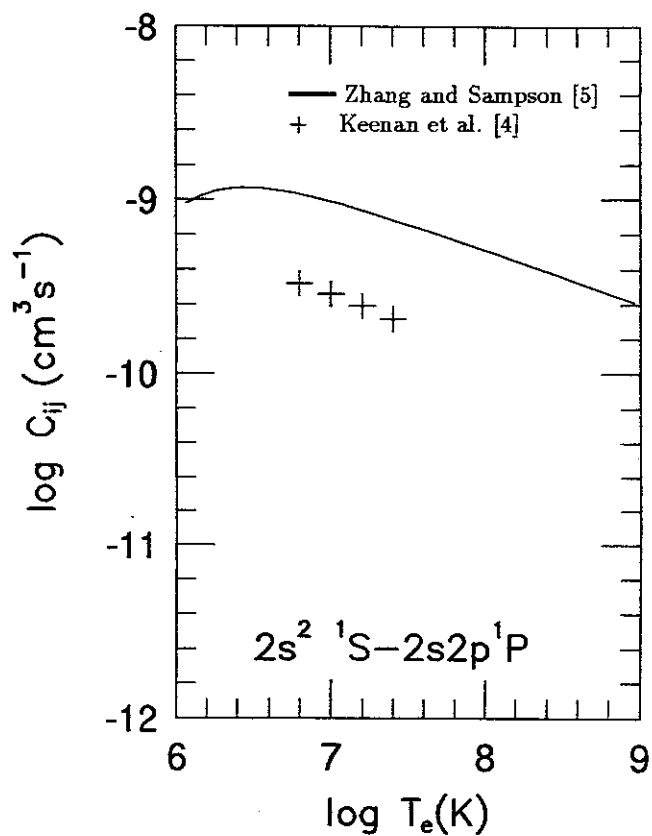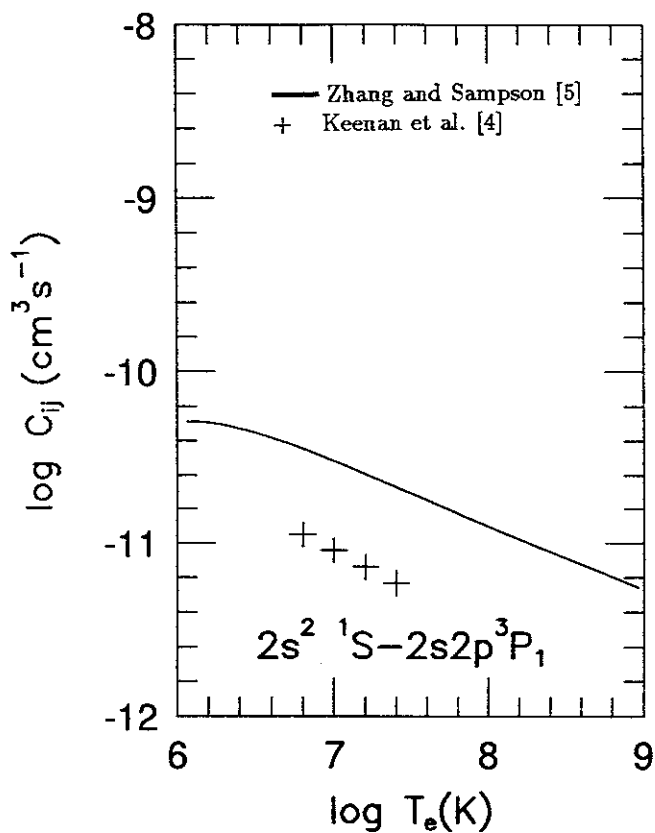
Fig. 1 (a)

Fig. 1 (b)

Fig. 2 (a)

Fig. 2 (b)

Fig. 3 (a)

Emissivity $(5.0 \times 10^{-11} \text{photons cm}^3 \text{s}^{-1} \text{Å}^{-1})$

λ (Å)

$2s^2\, {}^1S - 2s2p\, {}^1P$

$2s2p\, {}^3P_2 - 2p^2\, {}^1D_2$

$2s2p\, {}^3P_1 - 2p^2\, {}^3P_2$

$2s2p\, {}^3P_0 - 2p^2\, {}^3P_1$

$2s2p\, {}^1P - 2p^2\, {}^1S$

$2s2p\, {}^3P_1 - 2p^2\, {}^3P_1$

$2s2p\, {}^3P_2 - 2p^2\, {}^3P_2$

$2s2p\, {}^3P_1 - 2p^2\, {}^3P_0$

$2s2p\, {}^3P_2 - 2p^2\, {}^3P_1$

$2s2p\, {}^1P - 2p^2\, {}^1D$

$2s^2\, {}^1S - 2s2p\, {}^3P_1$

Emissivity $(1.0 \times 10^{-9} \text{photons cm}^3\text{s}^{-1}\text{Å}^{-1})$

λ (Å)

$2s^2\ ^1S - 2s3p\ ^1P$

$2s^2\ ^1S - 2s3p\ ^3P_1$

$2s2p\ ^1P - 2p3p\ ^1D$

$2s2p\ ^3P_1 - 2s3d\ ^1D$

$2s2p\ ^3P_0 - 2s3d\ ^3D_1$

$2s2p\ ^3P_1 - 2s3d\ ^3D_2$

$2s2p\ ^3P_1 - 2s3d\ ^3D_1$

$2s2p\ ^3P_2 - 2s3d\ ^3D_3$

$2s2p\ ^3P_2 - 2s3d\ ^3D_2$

$2s2p\ ^1P - 2s3d\ ^1D$

$2s2p\ ^3P_2 - 2s3s\ ^3S_1$

$2p^2\ ^1S - 2p3d\ ^1P$

$2p^2\ ^1D - 2p3s\ ^1P$

$2p^2\ ^3P_2 - 2p3s\ ^3P_1$

$2s2p\ ^1P - 2s3s\ ^1S$

$2p^2\ ^3P_1 - 2s3p\ ^3P_2$

$2p^2\ ^3P_1 - 2s3p\ ^3P_0$

$2p^2\ ^3P_2 - 2s3p\ ^3P_2$

$2p^2\ ^1D - 2s3p\ ^1P$

Fig. 3 (b)

Fig. 3 (c)

Emissivity (1.0×10^{-10} photons cm^{3}s^{-1}Å^{-1})

λ (Å)

$2s^2\ ^1S - 2s4p\ ^1P$

$2s^2\ ^1S - 2s4p\ ^3P_1$

$2s2p\ ^3P_0 - 2s4d\ ^3D_1$

$2s2p\ ^3P_1 - 2s4d\ ^3D_2$

$2s2p\ ^3P_2 - 2s4d\ ^3D_3$

$2s2p\ ^3P_2 - 2s4s\ ^3S_1$

$2s2p\ ^1P - 2s4d\ ^1D$

$2s2p\ ^1P - 2s4s\ ^1S$

$2p^2\ ^1S - 2s4p\ ^1P$

Fig. 4

Fig. 5 (a)

Fig. 5 (b)

Fig. 6 (a)

Fig. 6 (b)

Fig. 6 (c)

Fig. 7

Fig. 8 (a)(b)

R₃: I(267.62)/I(219.42)

R₄: I(267.62)/I(146.21)

R_3: $I(267.62)/I(219.42)$

R_4: $I(267.62)/I(146.21)$

(c)

I(267.62)/I(976.78)

$I(267.62)/I(976.78)$
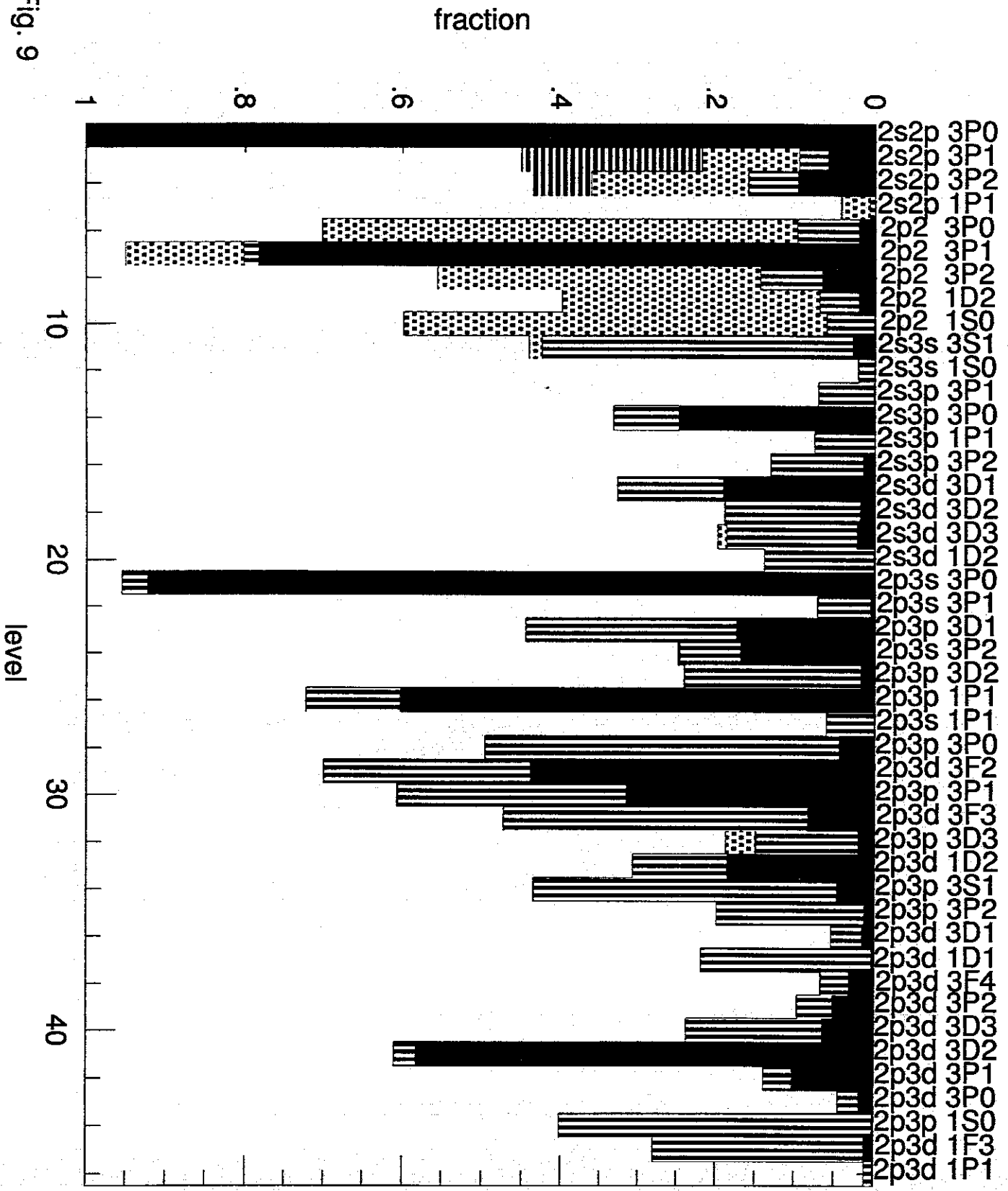
(d)
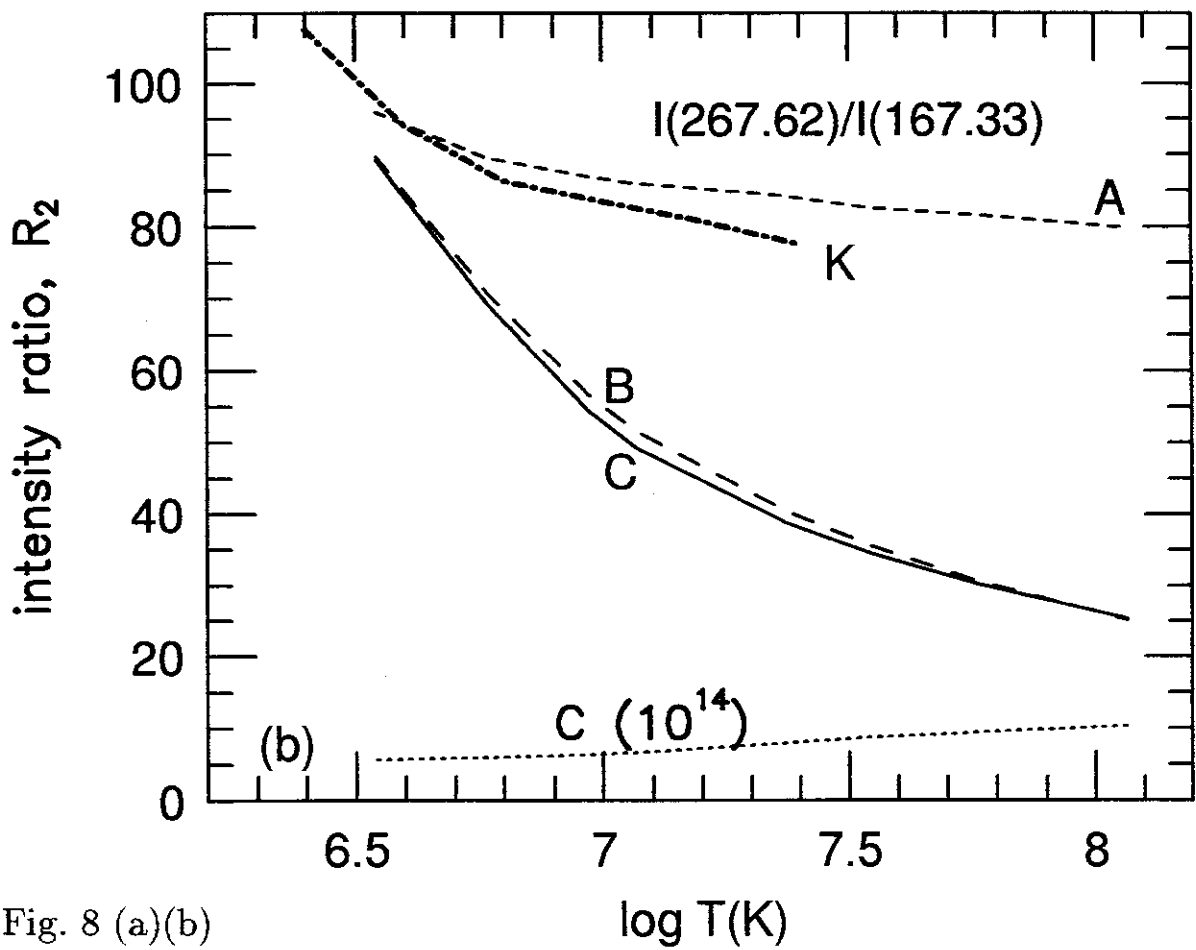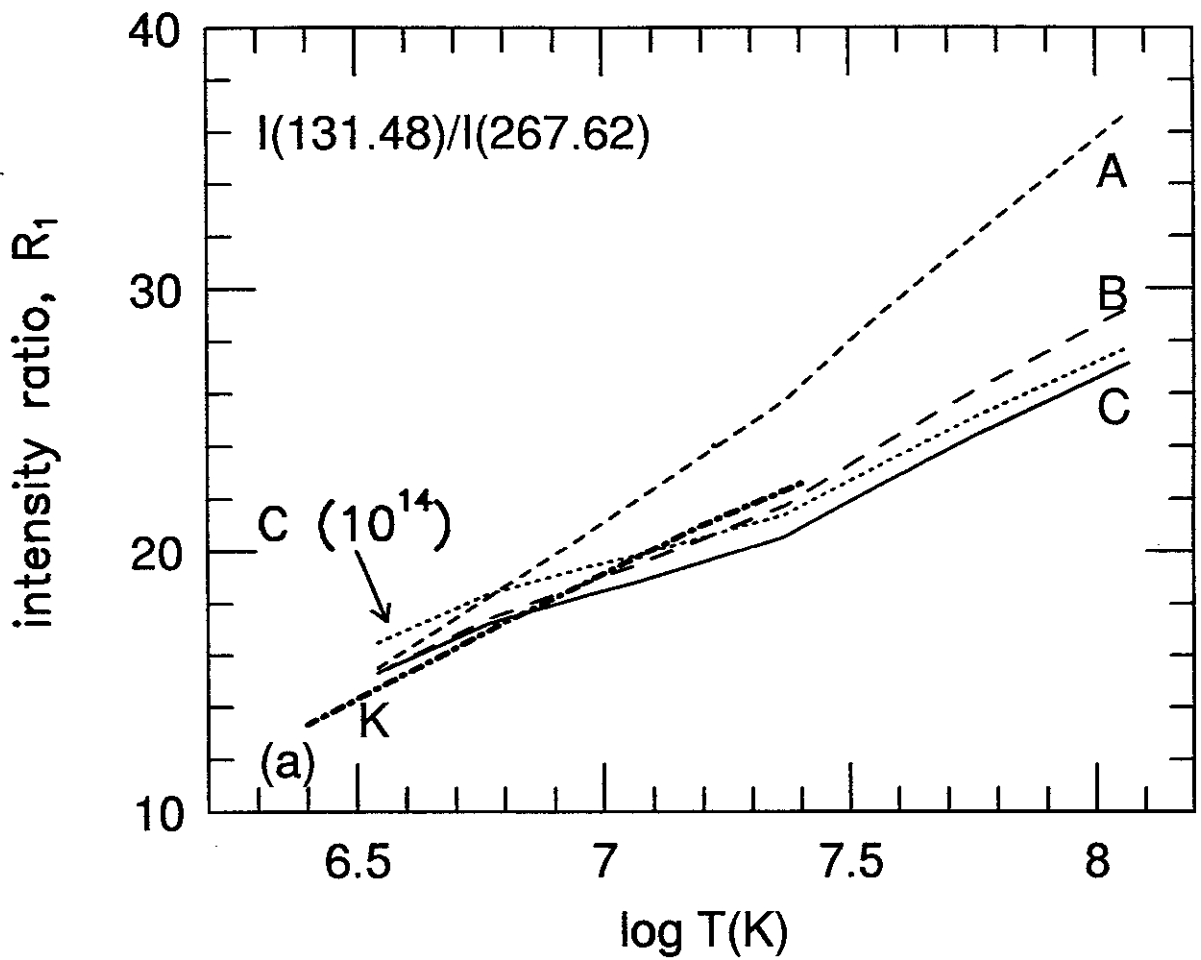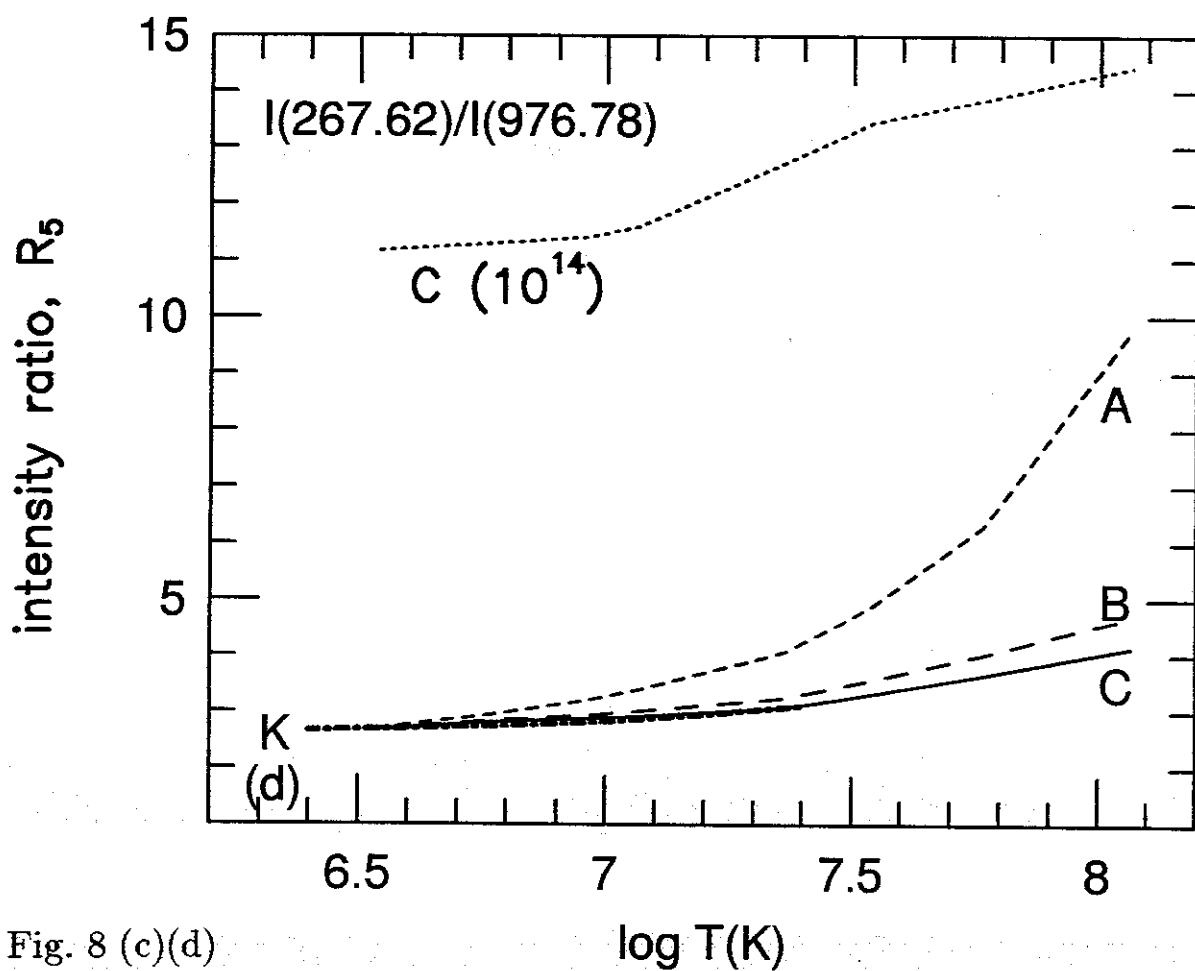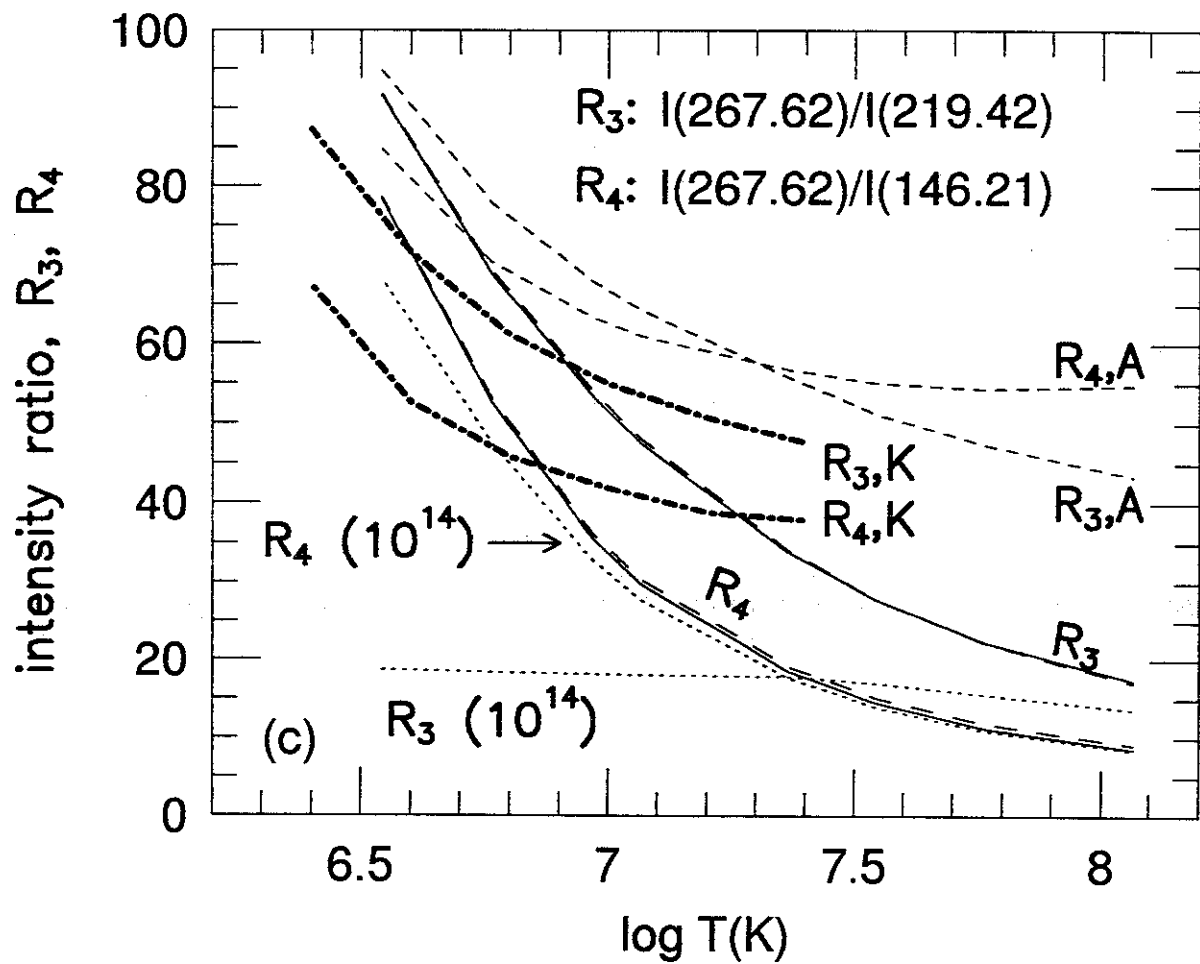
Fig. 8 (c)(d)
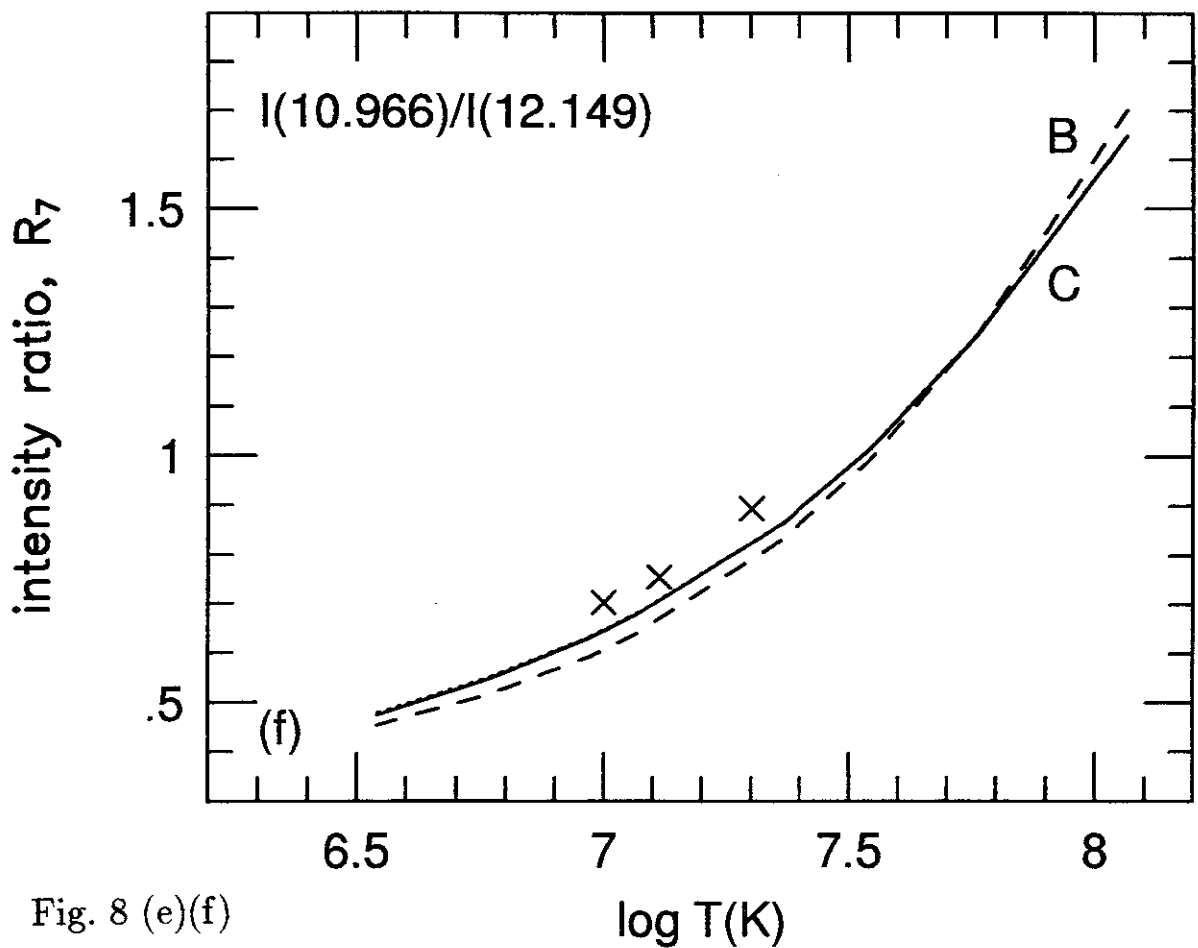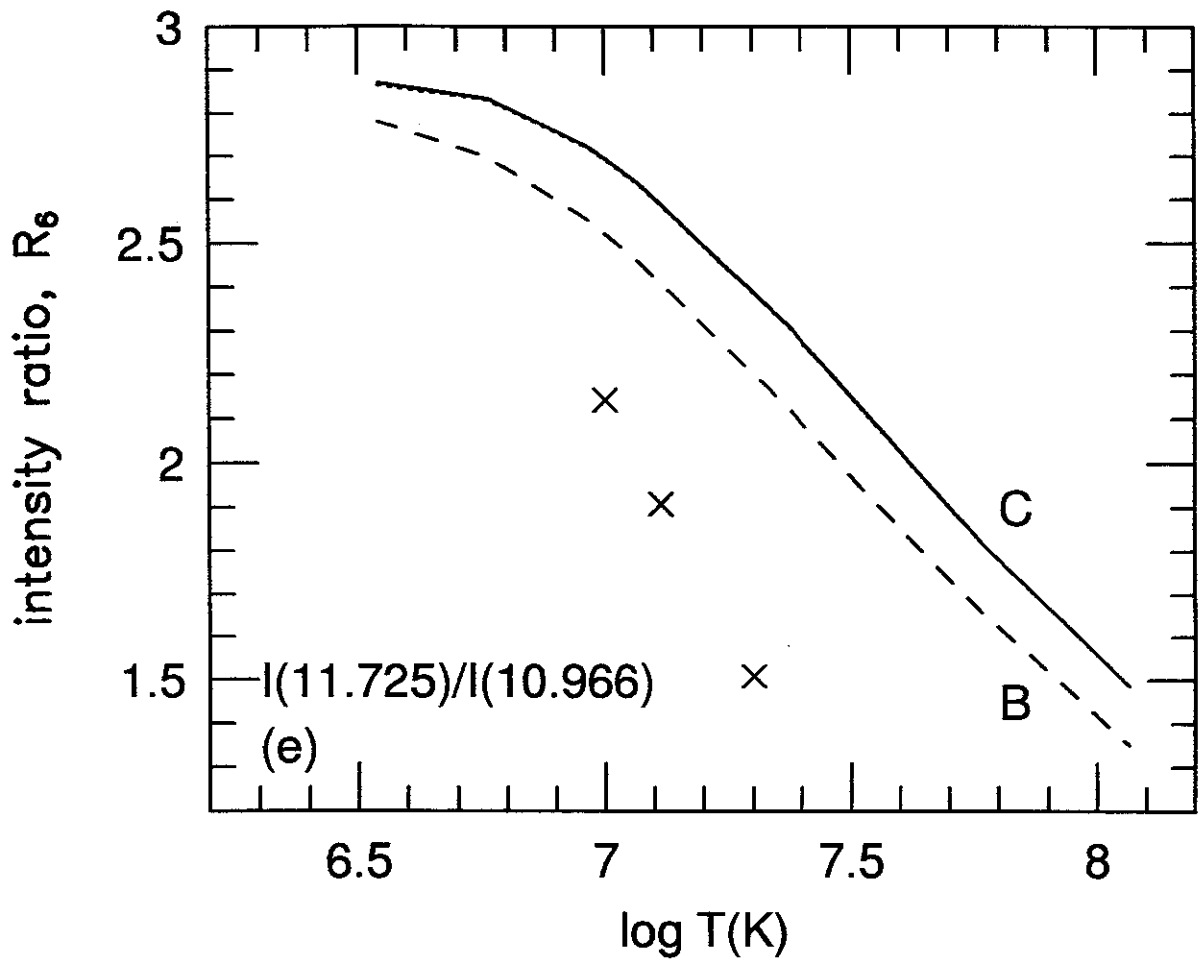
Fig. 8 (e)(f)
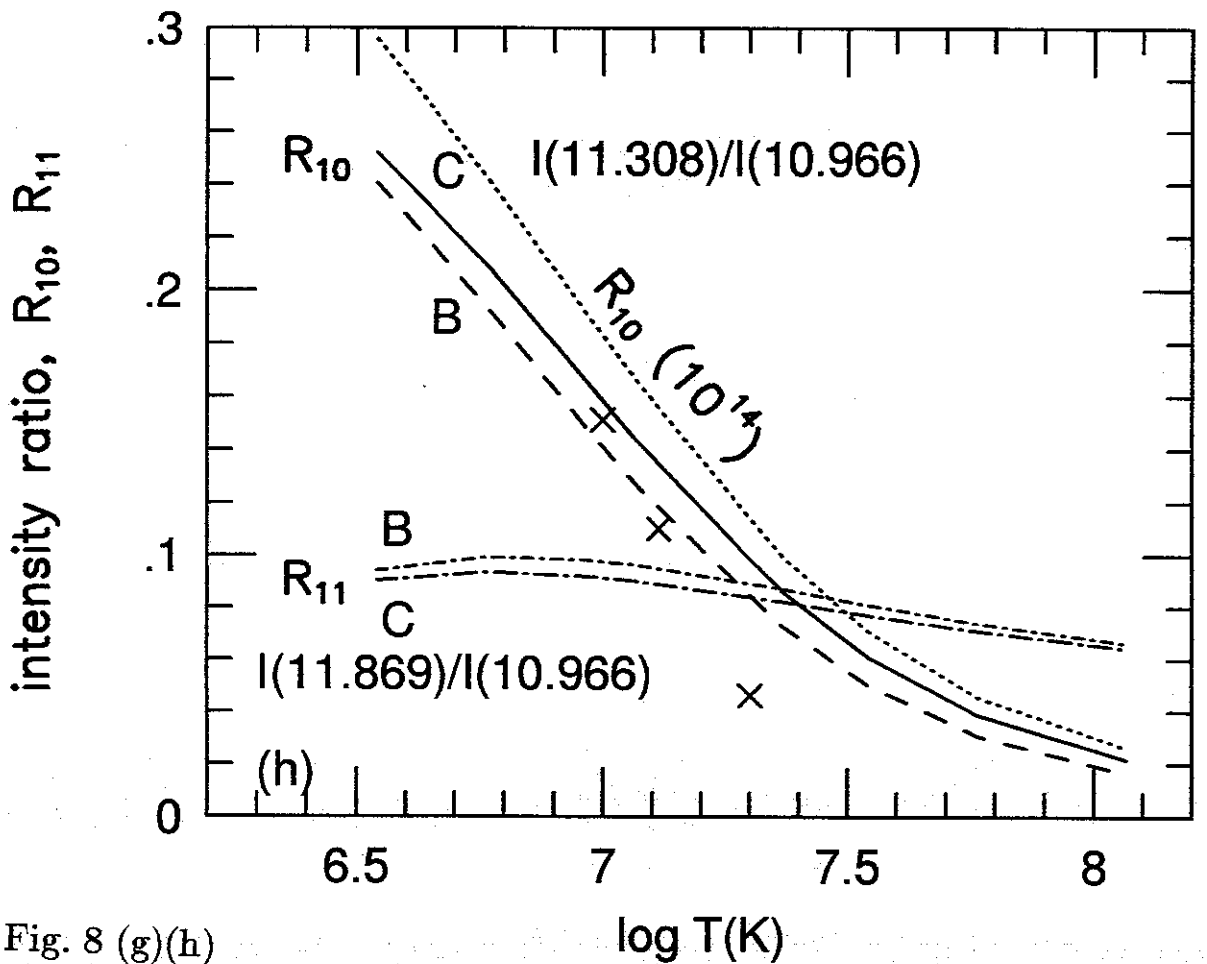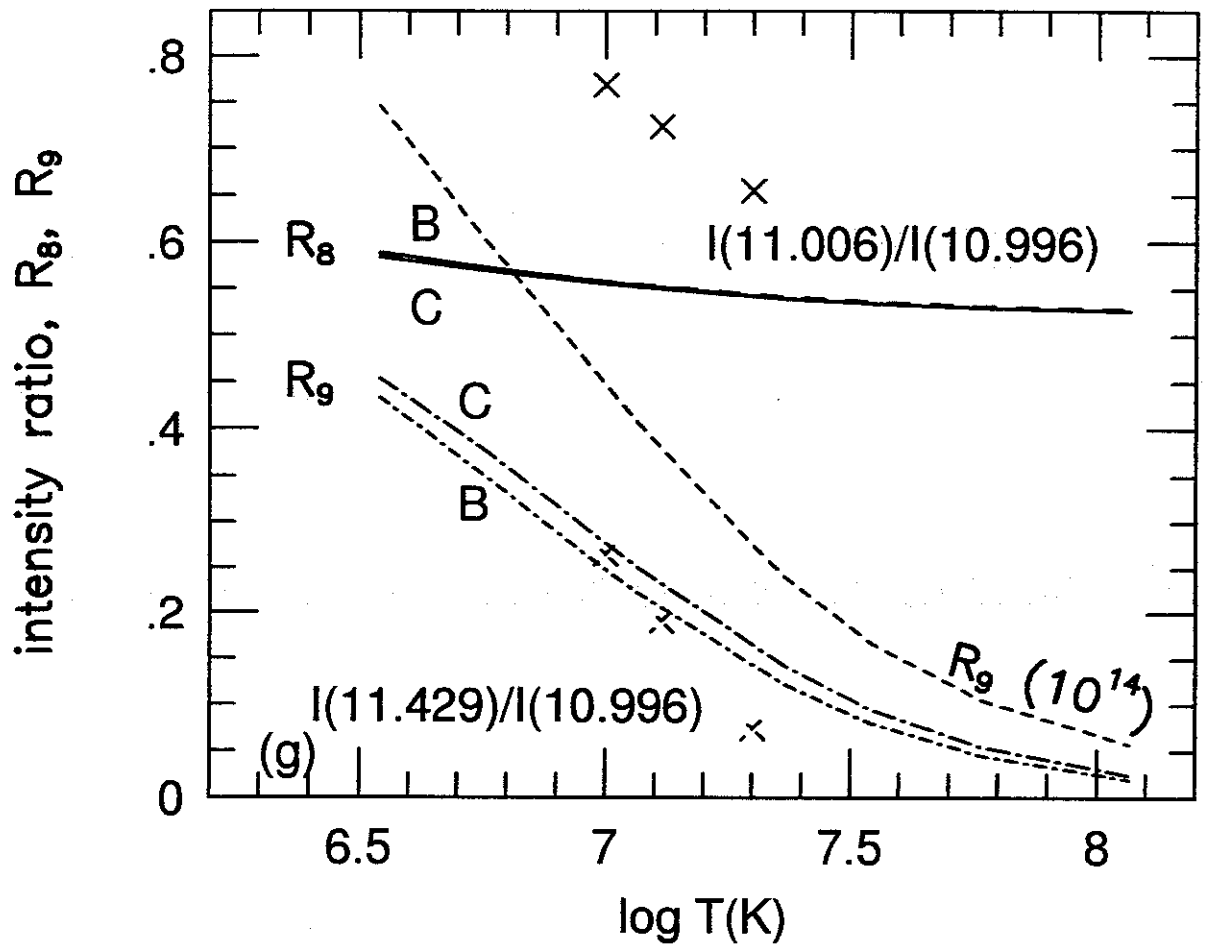
Fig. 8 (g)(h)
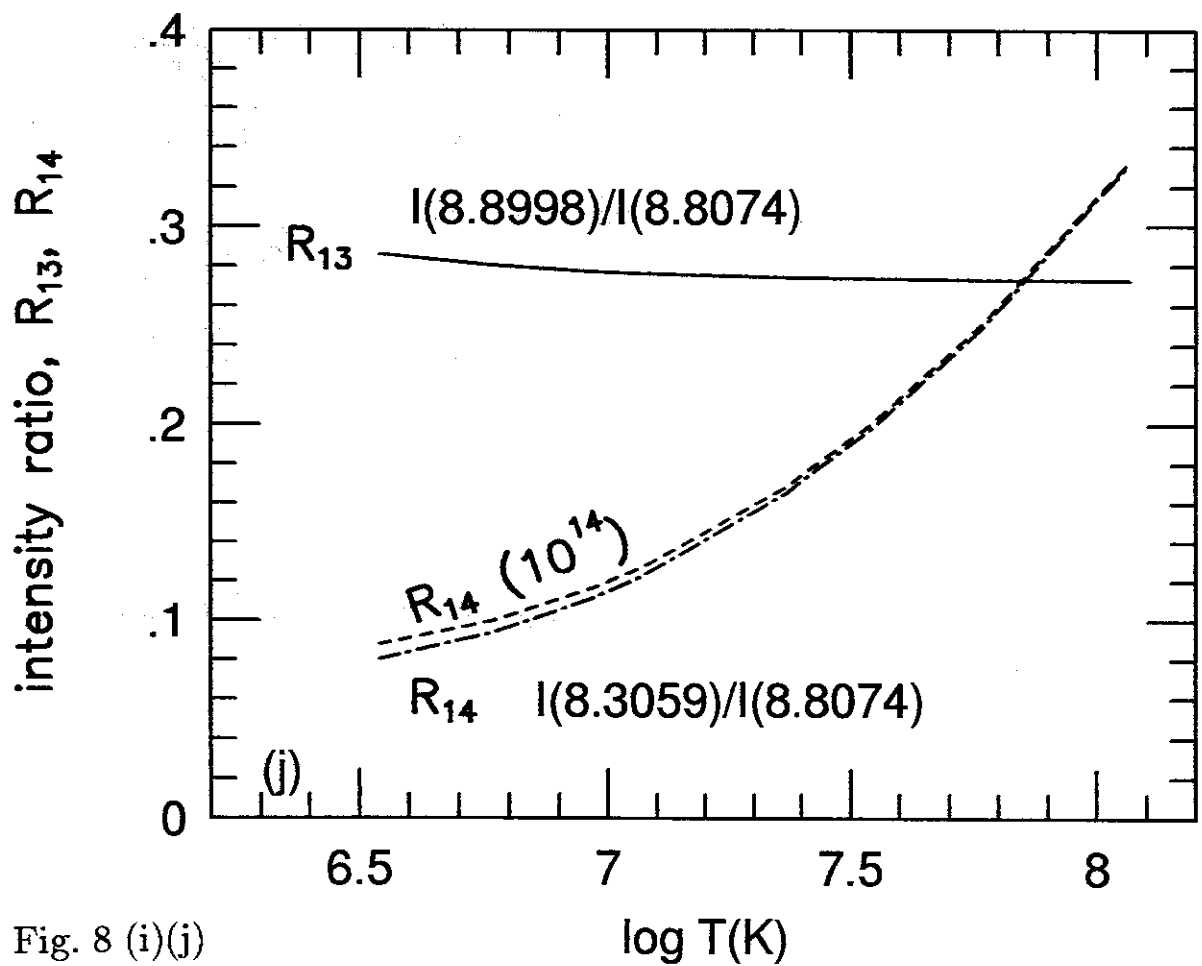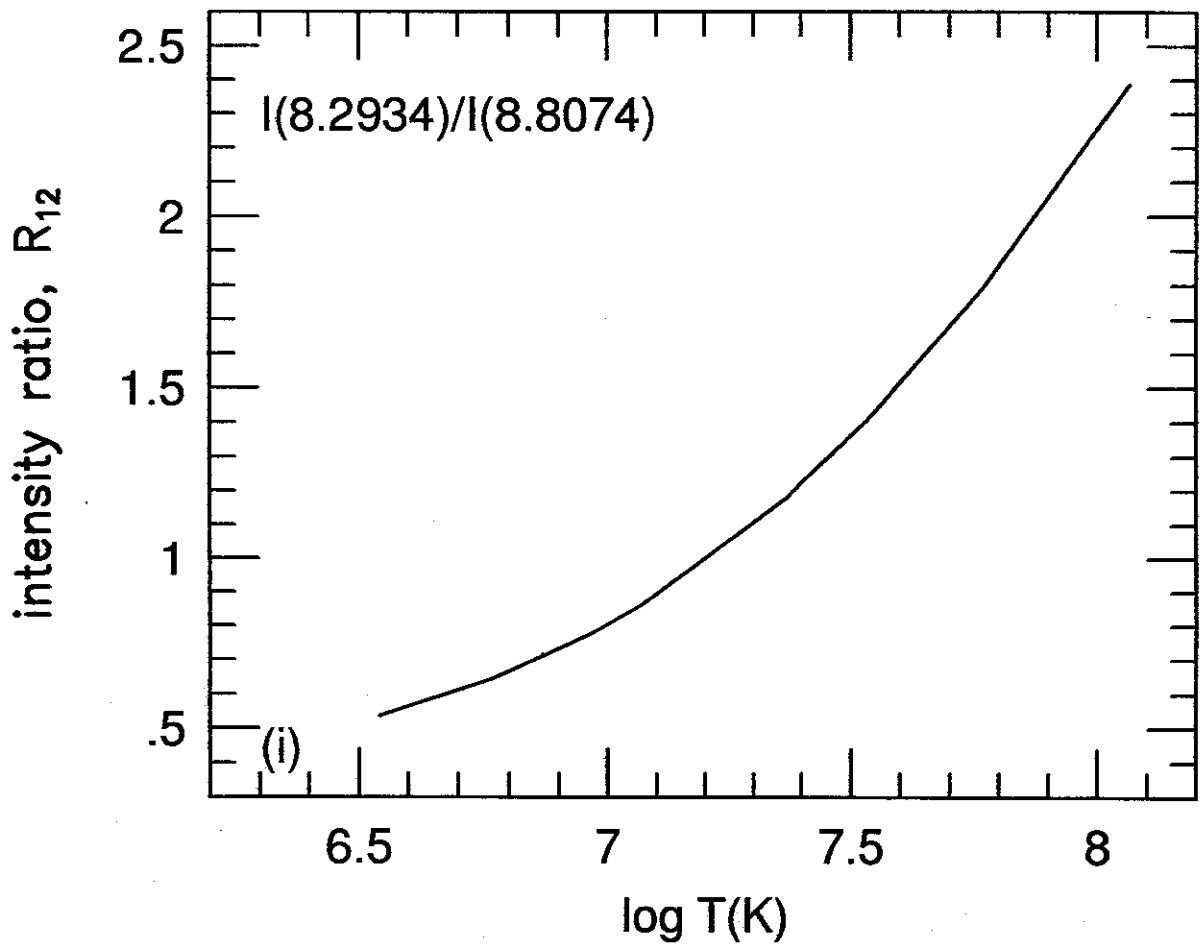
Fig. 8 (i)(j)

Fig. 9

Publication List of NIFS-DATA Series

NIFS-DATA-1 Y. Yamamura, T. Takiguchi and H. Tawara,
Data Compilation of Angular Distributions of Sputtered Atoms;
Jan. 1990

NIFS-DATA-2 T. Kato, J. Lang and K. E. Berrington,
*Intensity Ratios of Emission Lines from OV Ions for Temperature
and Density Diagnostics* ; Mar. 1990 [At Data and Nucl Data Tables
44(1990)133]

NIFS-DATA-3 T. Kaneko,
Partial Electronic Straggling Cross Sections of Atoms for Protons
;Mar. 1990

NIFS-DATA-4 T. Fujimoto, K. Sawada and K. Takahata,
*Cross Section for Production of Excited Hydrogen Atoms
Following Dissociative Excitation of Molecular Hydrogen by
Electron Impact* ; Mar. 1990

NIFS-DATA-5 H. Tawara,

*Some Electron Detachment Data for H⁻ Ions in Collisions with
Electrons, Ions, Atoms and Molecules − an Alternative Approach to
High Energy Neutral Beam Production for Plasma Heating−;*
Apr. 1990

NIFS-DATA-6 H. Tawara, Y. Itikawa, H. Nishimura, H. Tanaka and Y. Nakamura,
Collision Data Involving Hydro-Carbon Molecules; July 1990
[Supplement to Nucl. Fusion 2(1992)25]

NIFS-DATA-7 H.Tawara,
*Bibliography on Electron Transfer Processes in Ion-
Ion/Atom/Molecule Collisions −Updated 1990−;* Aug. 1990

NIFS-DATA-8 U.I.Safronova, T.Kato, K.Masai, L.A.Vainshtein and A.S.Shlyapzeva,
*Excitation Collision Strengths, Cross Sections and Rate
Coefficients for OV, SiXI, FeXXIII, MoXXXIX by Electron Impact
($1s^22s^2$-$1s^22s2p$-$1s^22p^2$ Transitions)* Dec.1990

NIFS-DATA-9 T.Kaneko,
*Partial and Total Electronic Stopping Cross Sections of Atoms and
Solids for Protons;* Dec. 1990

NIFS-DATA-10 K.Shima, N.Kuno, M.Yamanouchi and H.Tawara,
*Equilibrium Charge Fraction of Ions of Z=4-92 (0.02-6 MeV/u) and
Z=4-20 (Up to 40 MeV/u) Emerging from a Carbon Foil;* Jan.1991
[AT.Data and Nucl. Data Tables 51(1992)173]

NIFS-DATA-11   T. Kaneko, T. Nishihara, T. Taguchi, K. Nakagawa, M. Murakami,
M. Hosono, S. Matsushita, K. Hayase, M.Moriya, Y.Matsukuma,
K.Miura and Hiro Tawara,
*Partial and Total Electronic StoppingCross Sections of Atoms for a
Singly Charged Helium Ion: Part 1;*Mar. 1991

NIFS-DATA-12   Hiro Tawara,
*Total and Partial Cross Sections of Electron Transfer Processes for
Be^{q+} and B^{q+} Ions in Collisions with H, H_2 and He Gas Targets -
Status in 1991-;* June 1991

NIFS-DATA-13   T. Kaneko, M. Nishikori, N. Yamato, T. Fukushima, T. Fujikawa,
S. Fujita, K. Miki, Y. Mitsunobu, K. Yasuhara, H. Yoshida and
Hiro Tawara,
*Partial and Total Electronic Stopping Cross Sections of Atoms for a
Singly Charged Helium Ion : Part II;* Aug. 1991

NIFS-DATA-14   T. Kato, K. Masai and M. Arnaud,
*Comparison of Ionization Rate Coefficients of Ions from Hydrogen
through Nickel ;* Sep. 1991

NIFS-DATA-15   T. Kato, Y. Itikawa and K. Sakimoto,
*Compilation of Excitation Cross Sections for He Atoms by Electron
Impact;* Mar. 1992

NIFS-DATA-16   T. Fujimoto, F. Koike, K. Sakimoto, R. Okasaka, K. Kawasaki,
K. Takiyama, T. Oda and T. Kato,
Atomic Processes Relevant to Polarization Plasma Spectroscopy ;
Apr. 1992

NIFS-DATA-17   H. Tawara,
*Electron Stripping Cross Sections for Light Impurity Ions in
Colliding with Atomic Hydrogens Relevant to Fusion Research;*
Apr. 1992

NIFS-DATA-18   T. Kato,
*Electron Impact Excitation Cross Sections and Effective Collision
Strengths of N Atom and N-Like Ions -A Review of Available Data
and Recommendations- ;* Sep. 1992

NIFS-DATA-19   Hiro Tawara,
*Atomic and Molecular Data for H_2O, CO & CO_2 Relevant to Edge
Plasma Impurities,* Oct. 1992

NIFS-DATA-20   Hiro. Tawara,
*Bibliography on Electron Transfer Processes in Ion-
Ion/Atom/Molecule Collisions -Updated 1993-;* Apr. 1993

NIFS-DATA-21   J. Dubau and T. Kato,
                 Dielectronic Recombination Rate Coefficients to the Excited
                 States of C I from C II; Aug. 1994

NIFS-DATA-22   T. Kawamura, T. Ono, Y. Yamamura,
                 Simulation Calculations of Physical Sputtering and Reflection
                 *Coefficient of Plasma-Irradiated Carbon Surface;*Aug. 1994

NIFS-DATA-23   Y. Yamamura and H. Tawara,
                 Energy Dependence of Ion-Induced Sputtering Yields from
                 Monoatomic Solids at Normal Incidence; Mar. 1995

NIFS-DATA-24   T. Kato, U. Safronova, A. Shlyaptseva, M. Cornille, J. Dubau,
                 Comparison of the Satellite Lines of H-like and He-like Spectra;
                 Apr. 1995

NIFS-DATA-25   H. Tawara,
                 Roles of Atomic and Molecular Processes in Fusion Plasma
                 Researches - from the cradle (plasma production) to the grave
                 (after-burning) -; May 1995

NIFS-DATA-26   N. Toshima and H. Tawara
                 Excitation, Ionization, and Electron Capture Cross Sections of
                 Atomic Hydrogen in Collisions with Multiply Charged Ions;
                 July 1995

NIFS-DATA-27   V.P. Shevelko, H. Tawara and E.Salzborn,
                 Multiple-Ionization Cross Sections of Atoms and Positive Ions by
                 Electron Impact; July 1995

NIFS-DATA-28   V.P. Shevelko and H. Tawara,
                 Cross Sections for Electron-Impact Induced Transitions Between
                 Excited States in He: n, n'=2,3 and 4; Aug. 1995

NIFS-DATA-29   U.I. Safronova, M.S. Safronova and T. Kato,
                 Cross Sections and Rate Coefficients for Excitation of $\Delta n = 1$
                 Transitions in Li-like Ions with 6<Z<42; Sep. 1995

NIFS-DATA-30   T. Nishikawa, T. Kawachi, K. Nishihara and T. Fujimoto,
                 Recommended Atomic Data for Collisional-Radiative Model of
                 Li-like Ions and Gain Calculation for Li-like Al Ions in the
                 Recombining Plasma; Sep. 1995

NIFS-DATA-31   Y. Yamamura, K. Sakaoka and H. Tawara,
                 Computer Simulation and Data Compilation of Sputtering Yield by
                 Hydrogen Isotopes ($^1H^+$, $^2D^+$, $^3T^+$) and Helium ($^4He^+$) Ion
                 Impact from Monatomic Solids at Normal Incidence; Oct. 1995

NIFS-DATA-32 T. Kato, U. Safronova and M. Ohira,
Dielectronic Recombination Rate Coefficients to the Excited States of CII from CIII; Feb. 1996

NIFS-DATA-33 K.J. Snowdon and H. Tawara,
Low Energy Molecule-Surface Interaction Processes of Relevance to Next-Generation Fusion Devices; Mar. 1996

NIFS-DATA-34 T. Ono, T. Kawamura, K. Ishii and Y. Yamamura,
Sputtering Yield Formula for B_4C Irradiated with Monoenergetic Ions at Normal Incidence; Apr. 1996

NIFS-DATA-35 I. Murakami, T. Kato and J. Dubau,
UV and X-Ray Spectral Lines of Be-Like Fe Ion for Plasma Diagnostics; Apr. 1996